

## LITHIUM-RICH GIANTS IN GLOBULAR CLUSTERS\*

EVAN N. KIRBY<sup>1</sup>, PURAGRA GUHATHAKURTA<sup>2</sup>, ANDREW J. ZHANG<sup>3,4</sup>, JERRY HONG<sup>5</sup>, MICHELLE GUO<sup>4,6</sup>, RACHEL GUO<sup>6</sup>,  
JUDITH G. COHEN<sup>1</sup>, KATIA CUNHA<sup>7,8</sup>

*Accepted to ApJ on 2016 January 14*

### ABSTRACT

Although red giants deplete lithium on their surfaces, some giants are Li-rich. Intermediate-mass asymptotic giant branch (AGB) stars can generate Li through the Cameron–Fowler conveyor, but the existence of Li-rich, low-mass red giant branch (RGB) stars is puzzling. Globular clusters are the best sites to examine this phenomenon because it is straightforward to determine membership in the cluster and to identify the evolutionary state of each star. In 72 hours of Keck/DEIMOS exposures in 25 clusters, we found four Li-rich RGB and two Li-rich AGB stars. There were 1696 RGB and 125 AGB stars with measurements or upper limits consistent with normal abundances of Li. Hence, the frequency of Li-richness in globular clusters is  $(0.2 \pm 0.1)\%$  for the RGB,  $(1.6 \pm 1.1)\%$  for the AGB, and  $(0.3 \pm 0.1)\%$  for all giants. Because the Li-rich RGB stars are on the lower RGB, Li self-generation mechanisms proposed to occur at the luminosity function bump or He core flash cannot explain these four lower RGB stars. We propose the following origin for Li enrichment: (1) All luminous giants experience a brief phase of Li enrichment at the He core flash. (2) All post-RGB stars with binary companions on the lower RGB will engage in mass transfer. This scenario predicts that 0.1% of lower RGB stars will appear Li-rich due to mass transfer from a recently Li-enhanced companion. This frequency is at the lower end of our confidence interval.

*Subject headings:* stars: abundances — stars: chemically peculiar — stars: evolution — globular clusters

### 1. INTRODUCTION

Lithium was created in the Big Bang at a concentration of about 0.5 parts per billion (Coc et al. 2012). Since then, many of the Universe’s Li nuclei have been destroyed in nuclear burning because Li is susceptible to proton capture at relatively low temperatures ( $T \gtrsim 2.5 \times 10^6$  K). Li burning occurs in the centers of stars, but their surfaces are cool enough to preserve Li. Therefore, Li is observable only in stars with outer envelopes that have never been fully mixed down to high temperatures.

The atmospheres of most old, metal-poor stars on the main sequence display the same amount of Li (Spite & Spite 1982). This value,  $A(\text{Li}) \sim 2.2$ , is called the Spite plateau.<sup>9</sup> However, the plateau is sig-

nificantly below the primordial value,  $A(\text{Li}) = 2.72$  (Coc et al. 2012). Although the factor of 2–4 drop in Li abundance from the primordial value to the Spite plateau has been attributed to atomic diffusion and turbulent transport below the convection zone on the main sequence (Richard et al. 2005; Meléndez et al. 2010) and convective overshoot on the pre-main sequence (Fu et al. 2015), models of rotationally induced mixing (e.g., Pinsonneault et al. 1989) offer an explanation with less fine tuning. Pinsonneault et al. (1992, 1999, 2002) showed that calibrating mixing parameters to the Sun also explains Li depletion in other stars, including the mean and dispersion of the Li abundance on the Spite plateau. In addition, the rotation models also explain the behavior of other light elements, like Be and B (de la Reza et al. 1997; Deliyannis et al. 1998; Boesgaard et al. 2005).

In metal-rich stars, mixing more efficiently depletes surface lithium than in metal-poor stars (e.g., Meléndez et al. 2014; Tucci Maia et al. 2015). Furthermore, novae can generate Li for metal-rich, Population I stars (Romano et al. 1999; Tajitsu et al. 2015; Izzo et al. 2015). As a result, the Spite plateau breaks down at  $[\text{Fe}/\text{H}] \gtrsim -1.2$  (e.g., Chen et al. 2001). The constancy of Li on the Spite plateau makes Li anomalies in metal-poor stars readily apparent. For example, some carbon-rich stars show deficiencies in Li that can be explained by mass transfer from a binary, Li-depleted companion (Masseron et al. 2012).

However, it is more difficult to explain stars that are anomalous for being *enhanced* in Li. This is especially true for giant stars. Stars at the main sequence turn-off experience a rapid drop in Li abun-

of Li atoms and  $n(\text{H})$  is the number density of H atoms.

\* The data presented herein were obtained at the W. M. Keck Observatory, which is operated as a scientific partnership among the California Institute of Technology, the University of California and the National Aeronautics and Space Administration. The Observatory was made possible by the generous financial support of the W. M. Keck Foundation.

<sup>1</sup> California Institute of Technology, 1200 E. California Blvd., MC 249-17, Pasadena, CA 91125, USA

<sup>2</sup> UCO/Lick Observatory and Department of Astronomy and Astrophysics, University of California, 1156 High St., Santa Cruz, CA 95064, USA

<sup>3</sup> The Harker School, 500 Saratoga Ave., San Jose, CA 95129, USA

<sup>4</sup> Stanford University, 450 Serra Mall, Stanford, CA 94305, USA

<sup>5</sup> Palo Alto High School, 50 Embarcadero Rd., Palo Alto, CA, 94301, USA

<sup>6</sup> Irvington High School, 41800 Blacow Rd., Fremont, CA 94538, USA

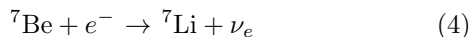
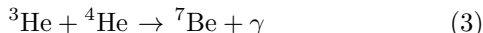
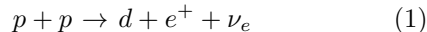
<sup>7</sup> Observatório Nacional, São Cristóvão Rio de Janeiro, Brazil

<sup>8</sup> University of Arizona, Tucson, AZ 85719, USA

<sup>9</sup>  $A(\text{Li}) = 12 + \log n(\text{Li})/n(\text{H})$ , where  $n(\text{Li})$  is the number density

dance (Pilachowski et al. 1993; Ryan & Deliyannis 1995; Lind et al. 2009b). As a low-mass star evolves on to the red giant branch (RGB), its surface convection zone deepens enough to dredge up material that has been processed through nuclear fusion, including Li burning. Although those regions are no longer hot enough to burn Li, they were once hot enough to do so. Hence, the dredge-up brings up Li-depleted material while Li on the surface is subducted into the star. The dredge-up dilutes the surface Li abundance to 5–10% of its original value. Models of dilution caused by the dredge-up (Deliyannis et al. 1990) explain the surface abundance of Li as a function of the sub-giant’s increasing luminosity or decreasing temperature. When the star reaches a luminosity of  $M_V \sim 0$ , the hydrogen-burning shell expands beyond the molecular weight boundary established by the first dredge-up (Iben 1968). “Extra” mixing—possibly thermohaline mixing (Charbonnel & Zahn 2007; Charbonnel & Lagarde 2010; Denissenkov 2010; Wachlin et al. 2011; Angelou et al. 2012; Lattanzio et al. 2015)—beyond the canonical stellar model changes the surface composition for stars at the RGB bump. This mixing rapidly destroys any Li remaining in the red giant’s atmosphere.

Nonetheless, some giants are Li-rich (see Wallerstein & Conti 1969). Cameron (1955) and Cameron & Fowler (1971) suggested a mechanism (the “Cameron–Fowler conveyor”) for producing excess Li in the atmospheres of giant stars. The central nuclear processes for the conveyor comprise the  $pp$ -II chain of hydrogen burning.



Reaction 3 is very active (compared to the  $pp$ -I chain) at temperatures around  $2 \times 10^7$  K. Li destruction, reaction 5, is very efficient at  $T \gtrsim 2.5 \times 10^6$  K. Hence,  ${}^7\text{Li}$  will be destroyed as soon as it is created in reaction 4 unless  ${}^7\text{Be}$  can be brought to cooler temperatures before it captures an electron. Although the half-life for reaction 4 is 53 days under terrestrial conditions, Cameron (1955) theorized that the scarcity of bound K-shell electrons available for reaction 4 at  $T > 10^6$  K, where  ${}^7\text{Be}$  is almost entirely ionized, extends the half-life to 50–100 years.

The mixing that accompanies thermal pulses in intermediate-mass stars on the second-ascent asymptotic giant branch (AGB) is deep enough to reach the  $pp$ -II burning zone. As a result, the Cameron–Fowler conveyor is a plausible explanation for Li-rich AGB stars in the mass range 4–7  $M_\odot$  (Sackmann & Boothroyd 1992). In fact, Li-rich AGB stars are not uncommon (Plez et al. 1993; Smith et al. 1995). However, the convective envelopes of first-ascent RGB stars and less massive AGB stars are not deep enough to activate the conveyor. Any excess Li in RGB stars must be a result of processes outside of “standard” stellar evolution of single stars with ordinary rotation rates. Sackmann & Boothroyd (1999)

called this non-standard phenomenon extra deep mixing combined with “cool bottom processing.” The mechanism for the mixing remains elusive.

Nonetheless, Li-rich red giants do exist. Kraft et al. (1999) discovered a luminous red giant with  $A(\text{Li}) = 3.0$  in the globular cluster (GC) M3. The star is unremarkable except for having over 1000 times more Li than it should have, based on its position on the RGB. Other GCs with Li-rich giants include M5 (in a post-AGB Cepheid, Carney et al. 1998), NGC 362 (Smith et al. 1999; D’Orazi et al. 2015b), and M68 (Ruchti et al. 2011). Kumar & Reddy (2009) and Kumar et al. (2011) found over a dozen Li-rich field K giants around solar metallicity. They also found tentative evidence for clustering of Li-rich giants around the red clump, or horizontal branch (HB), where stars burn helium in their cores after the He core flash at the tip of the RGB. The idea that the He core flash could activate the Cameron–Fowler conveyor was bolstered by Silva Aguirre et al.’s (2014) discovery of a Li-rich HB star whose He core burning was confirmed by asteroseismological measurements from the Kepler spacecraft (Gilliland et al. 2010). Monaco et al. (2014) also discovered a Li-rich, HB star in the open cluster Trumpler 5, and Anthony-Twarog et al. (2013) found a Li-rich giant in the open cluster NGC 6819 that is too faint to be on the HB or AGB. This star is particularly interesting for showing asteroseismic anomalies that could indicate rotationally induced mixing, which in turn could generate Li (e.g., Denissenkov 2012). Indeed, Carlberg et al. (2015) found that the star is rotating rapidly for a red giant, but puzzlingly, they did not find any additional evidence for deep mixing.

Metal-rich stars can have a complicated evolution of Li, as illustrated by the  $\sim 1.5$  dex scatter in Li abundance—even at fixed effective temperature—in Delgado Mena et al.’s (2015) survey of lithium in open clusters. Surveys for Li enhancement among metal-poor stars can be easier to interpret. Inspired by Kraft et al.’s (1999) discovery of a Li-rich giant in a metal-poor GC, Pilachowski et al. (2000) surveyed 261 giants in four metal-poor GCs, but they found no Li-rich giants. Therefore, the frequency of Li-rich red giants in GCs is less than 0.4%. D’Orazi et al. (2014, 2015a) also surveyed red giants in GCs and found one Li-rich giant out of about 350 giants, corresponding to a Li-rich frequency of  $(0.3 \pm 0.3)\%$ . Ruchti et al. (2011) searched for Li-rich giants in the Milky Way (MW) halo in the Radial Velocity Experiment (RAVE, Steinmetz et al. 2006). They found eight Li-rich giants out of 700 metal-poor field giants. They also found one Li-rich giant in the GC M68. Domínguez et al. (2004) and Kirby et al. (2012) also found 15 Li-rich giants in MW dwarf satellite galaxies. However, the MW field and dwarf galaxies are not amenable to easily distinguishing between the AGB and upper RGB. In fact, many of the Li-rich giants discovered by Ruchti et al. (2011) and Kirby et al. (2012) could be AGB stars.

Explanations for Li-rich RGB stars fall into three categories: engulfment of a substellar companion, self-generation, and mass transfer. In the engulfment scenario (e.g., Siess & Livio 1999; Denissenkov & Weiss 2000; Melo et al. 2005; Villaver & Livio 2009; Adamów et al. 2012), a red giant expands into the orbit of a rocky planet, a hot Jupiter, or a compan-

ion brown dwarf. The destroyed companion could potentially enrich the star with Li and other volatile elements that concentrate in planets (Carlberg et al. 2013). Even if the engulfed companion does not donate Li to its host star, it would provide angular momentum. The resulting increase in rotation rate could itself inspire deep mixing that activates the Cameron–Fowler conveyor (Denissenkov & Herwig 2004).

In the self-generation scenario, stars can experience deep mixing events that dredge Li to the stellar surface, where it is observable. Rotationally induced mixing is one example. Indeed, some Li-rich giants are rapid rotators (Drake et al. 2002; Guillout et al. 2009; Carlberg et al. 2010), but others are not (Ruchti et al. 2011). Other possible causes are mixing at the RGB luminosity function bump (Charbonnel & Balachandran 2000) or deep mixing inspired by He core flashes at the tip of the RGB or on the HB (Kumar et al. 2011; Silva Aguirre et al. 2014; Monaco et al. 2014). For example, D’Orazi et al. (2015b) found a Li-rich giant in the GC NGC 362 that may be either at the RGB bump (hydrogen shell burning) or on the red clump (helium core burning). On the other hand, Anthony-Twarog et al.’s (2013) Li-rich giant in NGC 6819 is one counter-example below the RGB bump. The chemical analysis of that star by Carlberg et al. (2015) found no evidence for deep mixing in any element other than Li. Furthermore, most deep mixing scenarios predict that the Li-rich giants would cluster at a specific evolutionary phase (luminosity). However, Lebzelter et al. (2012) found no luminosity clustering of Li-rich red giants.

Finally, stars can alter their surface compositions through binary mass transfer. AGB stars are known to generate carbon and neutron-capture elements, like barium (Busso et al. 1995). Hence, binary companions to AGB stars or former AGB stars can be enhanced in those elements (McClure et al. 1980). Intermediate-mass AGB stars can also dredge up Li in the Cameron–Fowler conveyor. Even less massive AGB stars might be able to generate Li with the help of thermohaline mixing (Cantiello & Langer 2010). If the star transferred mass to a companion during a phase of Li dredge-up, then that companion would be enhanced in Li. This is a possible explanation for a Li-rich turn-off star in the GC NGC 6397 (Koch et al. 2011; Pasquini et al. 2014). That star will remain enhanced in Li until the first dredge-up. Assuming that the dredge-up dilutes a fixed percentage of Li for all stars of similar mass and composition, then the star would still appear Li-enhanced relative to other post-dredge-up stars in the cluster.

GCs are the best environments to study low-mass stellar evolution. The common distance to all the member stars makes it easy to determine stellar luminosity. The common age and small abundance dispersion in most elements implies a similar evolution for all stars. To first order, a GC is a snapshot of stellar evolution over a sequence of stellar masses at fixed age and mostly fixed metallicity. With reasonably attainable photometric uncertainty, the AGB and RGB can be distinguished with a color–magnitude diagram (CMD) except for the bright-end giants, where the AGB nearly merges with the RGB.

We exploited the controlled stellar populations of GCs to study the phenomenon of Li-rich giants. We searched for Li-rich giants and classified them photometrically as

RGB or AGB. Section 2 describes our observations, and Section 3 details the measurement of Li and other spectroscopic properties. In Section 4, we define what it means to be “Li-rich” and quantify the statistics of Li-rich giants in GCs. We address the possible origins of Li enhancement in Section 5, and we summarize our conclusions in Section 6.

## 2. SPECTROSCOPIC OBSERVATIONS

We observed 25 GCs with Keck/DEIMOS (Faber et al. 2003) over eight years. Table 1 lists the clusters and their coordinates. Some of these slitmasks were observed with the purpose of validating a method to measure metallicities and  $\alpha$  element abundances from DEIMOS spectra. Kirby et al. (2008, 2010) previously published these observations. Most of the remaining slitmasks were designed expressly to search for Li-rich red giants.

### 2.1. Source Catalogs

We used custom slitmasks designed to observe giant stars in the clusters. In order to design the slitmasks, we used photometric catalogs from various sources.

Our primary source of photometry was P.B. Stetson’s database of photometric standard fields. We downloaded some of these from Stetson’s public web page, but he provided some of these catalogs to us privately (see Kirby et al. 2010). Several of these clusters were also previously published (Stetson 1994, 2000). These catalogs were made with DAOPHOT (Stetson 1987, 2011), which models the point spread functions (PSFs) of stars. This approach performs better than aperture photometry in crowded fields, like GCs.

Some of Stetson’s clusters had dense sampling over a field comparable in size to a DEIMOS slitmask. In these cases, we relied on his photometry alone. The catalogs for other clusters sampled only tens or hundreds of stars for the purposes of providing a photometric calibration field rather than a science catalog. In these cases, we supplemented Stetson’s photometry with other sources. Table 1 lists the source catalogs for each cluster. Notable sources include the Sloan Digital Sky Survey (SDSS, Abazajian et al. 2009) and An et al. (2008). Because the primary SDSS catalog uses aperture photometry, An et al. (2008) re-reduced the photometry of select GCs with DAOPHOT.

All of the catalogs used have coverage in at least two of the three filters  $B$ ,  $V$ , and  $I$ . We corrected the observed magnitudes for extinction according to the dust maps of Schlegel et al. (1998).

### 2.2. Target Selection

We designed the slitmasks with a minimum slit length of  $4''$  and separation between slits of  $0''.35$ . These choices allowed just enough separation between stars to (1) avoid overlapping spectra and (2) permit sky subtraction from the empty portions of the slits. However, these restrictions also forced us to choose among the many stars in the dense GCs. Although several hundred GC giants might have been visible in a single DEIMOS pointing, the slitmask would allow only about 150 targets at most. We developed target selection strategies to pick out likely giant members of the GCs.

Because the 75 slitmasks were designed for different projects over many years, the target selection strategy

**Table 1**  
Globular Clusters Observed

| GC             | RA (J2000) | Dec (J2000) | Source Catalogs                     |
|----------------|------------|-------------|-------------------------------------|
| NGC 288        | 00 52 45   | -26 34 57   | Stetson; Bellazzini et al. (2001)   |
| Pal 2          | 04 46 05   | +31 22 53   | Stetson                             |
| NGC 1904 (M79) | 05 24 11   | -24 31 28   | Stetson; Rosenberg et al. (2000)    |
| NGC 2419       | 07 38 08   | +38 52 56   | Stetson (2000)                      |
| NGC 4590 (M68) | 12 39 27   | -26 44 38   | Stetson; Walker (1994)              |
| NGC 5024 (M53) | 13 12 55   | +18 10 05   | Stetson; An et al. (2008)           |
| NGC 5053       | 13 16 27   | +17 42 00   | Stetson; An et al. (2008)           |
| NGC 5272 (M3)  | 13 42 11   | +28 22 38   | Stetson (2000)                      |
| NGC 5634       | 14 29 37   | -05 58 35   | Stetson; Bellazzini et al. (2002)   |
| NGC 5897       | 15 17 24   | -21 00 36   | Stetson; Testa et al. (2001)        |
| NGC 5904 (M5)  | 15 18 33   | +02 04 51   | Stetson (2000); An et al. (2008)    |
| Pal 14         | 16 11 00   | +14 57 27   | Saha et al. (2005)                  |
| NGC 6205 (M13) | 16 41 41   | +36 27 35   | Stetson                             |
| NGC 6229       | 16 46 58   | +47 31 39   | SDSS                                |
| NGC 6341 (M92) | 17 17 07   | +43 08 09   | Stetson (2000); An et al. (2008)    |
| NGC 6656 (M22) | 18 36 23   | -23 54 17   | Stetson; Peterson & Cudworth (1994) |
| NGC 6779 (M56) | 19 16 35   | +30 11 00   | Hatzidimitriou et al. (2004)        |
| NGC 6838 (M71) | 19 53 46   | +18 46 45   | Stetson                             |
| NGC 6864 (M75) | 20 06 04   | -21 55 16   | Kravtsov et al. (2007)              |
| NGC 7006       | 21 01 29   | +16 11 14   | Stetson (2000); An et al. (2008)    |
| NGC 7078 (M15) | 21 29 58   | +12 10 01   | Stetson (1994, 2000)                |
| NGC 7089 (M2)  | 21 33 27   | -00 49 23   | Stetson (2000); An et al. (2008)    |
| NGC 7099 (M30) | 21 40 22   | -23 10 47   | Stetson; Sandquist et al. (1999)    |
| Pal 13         | 23 06 44   | +12 46 19   | Stetson                             |
| NGC 7492       | 23 08 26   | -15 36 41   | Stetson                             |

**References.** — Cluster coordinates are from the compilation of Harris (1996, updated 2010) and references therein. “Stetson” refers to photometry by P.B. Stetson. Most of the photometry is available at <http://www2.cadc-ccda.hia-ihp.nrc-cnrc.gc.ca/community/STETSON/standards/>, but Stetson provided some of it directly to us. “SDSS” refers to photometry from the Sloan Digital Sky Survey (Abazajian et al. 2009).

was not uniform. Although most masks were designed for giants, some included main sequence stars. In general, selection along the RGB was performed by defining selection regions in the CMD. In some cases, where the RGB was well-defined and distinct from the foreground, we drew an irregular polygon around the RGB and selected stars inside of it. In other cases, we drew an old ( $\sim 12$  Gyr) isochrone corresponding to the metallicity of the cluster (Harris 1996, updated 2010). We used both Victoria–Regina (VandenBerg et al. 2006) and Yonsei–Yale (Demarque et al. 2004) isochrone models. The selection region was defined within a color range (typically 0.1 mag) around the isochrone. For most slitmasks, brighter stars were given higher priority for selection.

The target selection favored first-ascent RGB stars rather than helium-burning stars on the HB or AGB. The HB was particularly disfavored because the spectra of hot, blue stars do not readily lend themselves to the measurement of radial velocity and metallicity, which was the original intent for many of the slitmasks. Therefore, this data set is not ideal to search for Li-richness on the HB. However, it is suitable for quantifying the frequency of Li-rich giants on the RGB or upper AGB.

Figure 1 shows the extinction- and reddening-corrected CMDs for all of the GCs in our sample. M53 and NGC 7492 are shown with  $(B - V)_0$  color, and all of the other GCs are shown with  $(V - I)_0$ . Stars that we identified as members (Section 3.3) are shown as colored points or black, five-pointed stars.

### 2.3. Separation of RGB and AGB

GCs are excellent laboratories to study stellar evolution because they are nearly single-age populations of nearly uniform metallicity.<sup>10</sup> For these reasons, GCs are the best stellar populations for distinguishing between the AGB and the RGB. This distinction helps determine how evolutionary phase plays a role in Li-richness.

Although model isochrones could be used for this task, we found that small imperfections in the models resulted in misidentification at high stellar luminosities, where the AGB asymptotically approaches the RGB. Instead, we identified the AGB “by eye.” We drew a selection region around the AGB for each GC. AGB stars are shown in blue in Figure 1. RGB stars are shown in red.

### 2.4. Observations

Table 2 lists the observing log, including the slitmask name, the number of targets on the slitmask, the date of observation, the airmass and seeing at the time of observation, the number of exposures, and the total exposure

<sup>10</sup> There is extensive observational evidence that GCs are chemically complex (e.g., Gratton et al. 2004, 2012). In particular, primordial intracluster variation in certain elements, such as O, Na, Mg, and Al, indicates that cluster stars were differentially enhanced with the products of high-temperature hydrogen burning. Li is not immune to the primordial variation, as exhibited by weak Li–Na and Li–Al anti-correlations observed in some clusters (Lind et al. 2009b; Monaco et al. 2012; D’Orazi et al. 2015a). Unfortunately, we cannot distinguish between first and later generation stars in our sample because we cannot observe Na in our spectra. However, GCs are still simple enough for our purposes. Specifically, it is straightforward to distinguish the AGB from the RGB, and the heavy elements, like Fe, are invariant within each of the clusters in our sample.

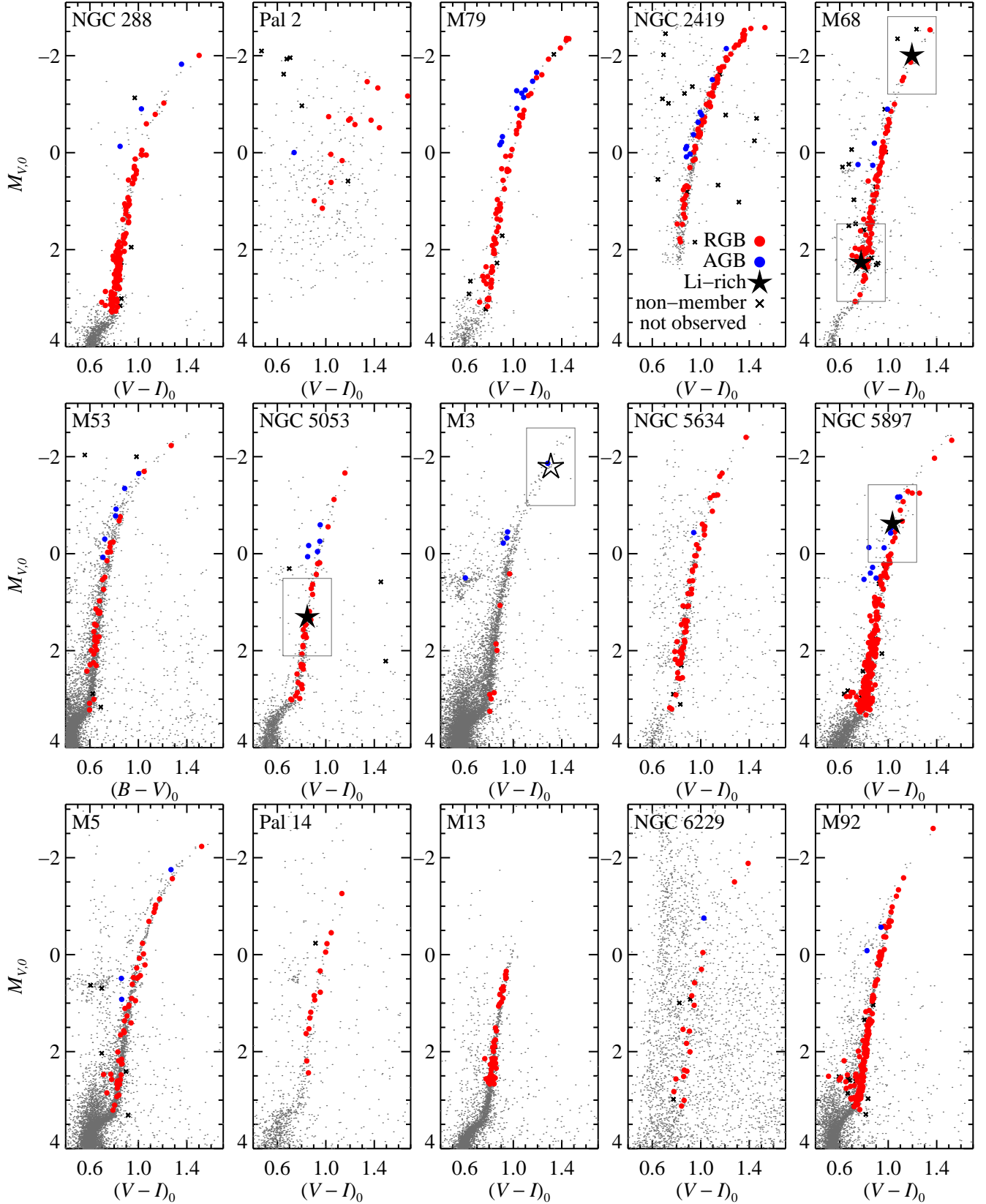


**Figure 1.** Color-magnitude diagrams for all 25 GCs observed with DEIMOS. The panel for NGC 2419 includes a figure legend. Li-rich stars are shown as black, five-pointed stars. The hollow star indicates the Li-rich giant IV-101 in M3 (Kraft et al. 1999), which is not part of our sample. Spectroscopically confirmed, Li-normal members are shown as red (RGB) and blue (AGB) points. Non-members are shown as black crosses. Gray points show stars that we did not observe with DEIMOS. We distinguished between RGB and AGB stars by drawing selection regions in the CMDs. Figure 5 shows detail of the gray boxes around the Li-rich stars.

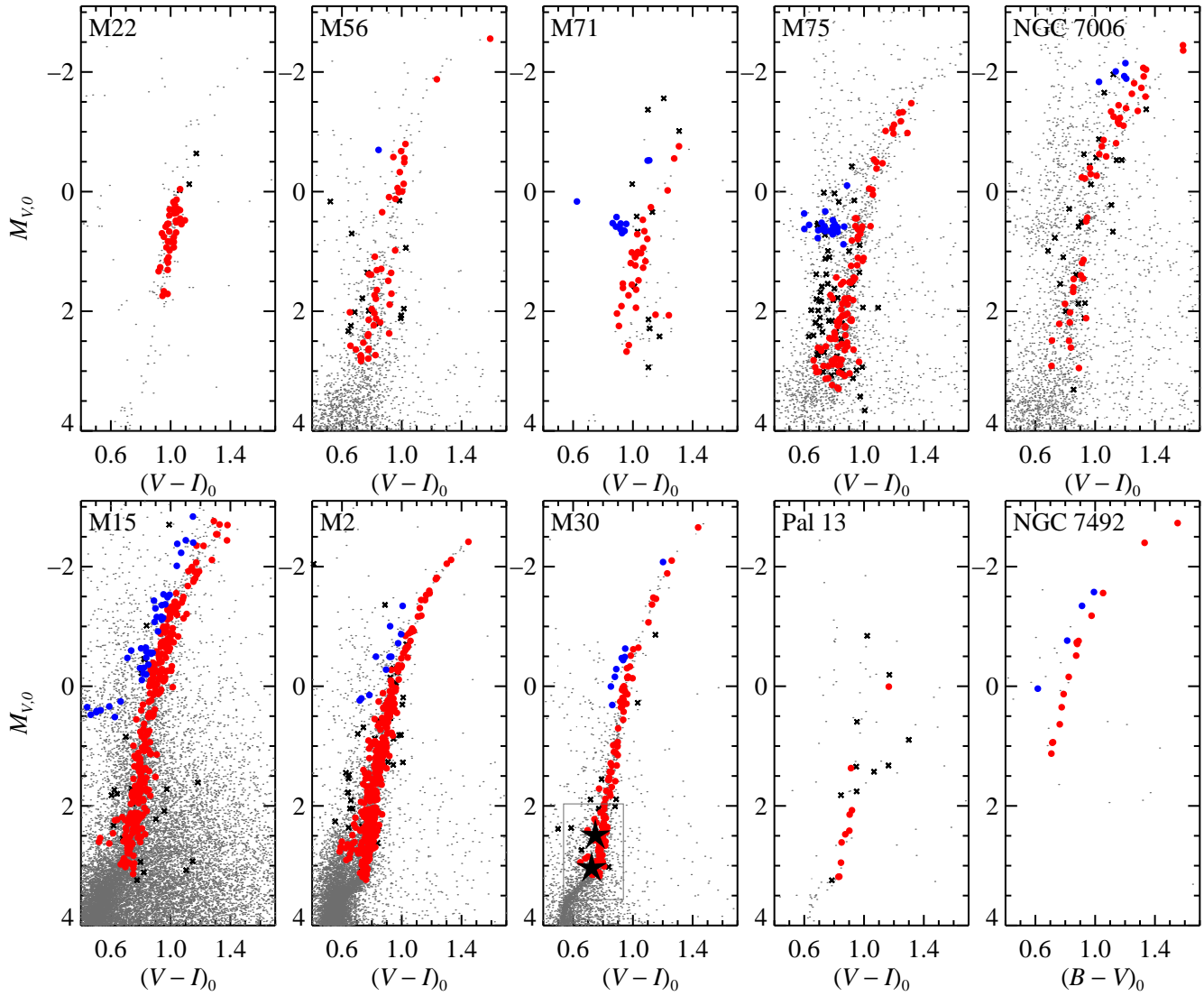


Figure 1. — *continued* —

time. The number of targets is the number of science slitlets in the mask (excluding alignment boxes). It is not the number of stars in the final sample. In addition to member giants, the slitmasks included main sequence stars as well as non-members.

All slitmasks were observed with the 1200G grating, which has a groove spacing of  $1200 \text{ mm}^{-1}$  and a blaze wavelength of  $7760 \text{ \AA}$ . The slit widths were typically  $0''.7$ . The resulting resolution was  $1.2 \text{ \AA}$ , which corresponds to a resolving power of  $R \approx 6500$  at the blaze wavelength. Each pixel encompasses  $0.33 \text{ \AA}$ , such that a resolution element spans 3.6 pixels. Slitmasks with the letter “l” were observed at a central wavelength of  $7500 \text{ \AA}$ . Other slitmasks were observed at a central wavelength of  $7800 \text{ \AA}$ . The OG550 order-blocking filter blocked second- and higher-order light from contaminating the spectra. We used DEIMOS’s flexure compensation system, which provides wavelength stability of about  $0.03 \text{ \AA}$  during the observation of one slitmask. Afternoon calibrations included exposures of a quartz lamp for flat fielding and an exposure of Ne, Kr, Ar, and Xe arc lamps for wavelength calibration.

We reduced the DEIMOS spectra with the `spec2d` IDL data reduction pipeline developed by the DEEP2 team (Cooper et al. 2012; Newman et al. 2013). The pipeline excises the 2-D spectrum for each slitlet. The 2-D spectrum is flat-fielded and wavelength-calibrated. The wavelength calibration from the arc lamps is refined with night sky emission lines. All of the exposures are combined, and cosmic rays are removed. Finally, the 1-D spectrum is extracted with optimal extraction. The software tracks the variance spectrum at every step. The result is a flat-fielded, wavelength-calibrated, 1-D spectrum of the target along with an estimate of the error in each pixel.

Figure 2 shows the spectra of the six giants that we determined to be Li-rich members of their respective GCs (see Section 4). Only a small spectral region around the  $\text{Li I } \lambda 6707$  line is shown.

### 3. SPECTROSCOPIC MEASUREMENTS

We measured four important parameters from each spectrum: radial velocity,  $v_{\text{helio}}$ ; effective temperature,  $T_{\text{eff}}$ ; metallicity,  $[\text{Fe}/\text{H}]$ ; and Li abundance,  $A(\text{Li})$ .

#### 3.1. Radial Velocities

We measured  $v_{\text{helio}}$  in the same manner as Simon & Geha (2007). First, we measured  $v_{\text{obs}}$ , the velocity required to shift the spectrum into the rest frame. To do so, we cross-correlated each spectrum with 16 template spectra observed with DEIMOS, kindly provided by Simon & Geha. Because of imperfect centering in the slitlet, a star can have an apparent radial velocity with respect to the telluric absorption lines. To counteract this error, we cross-correlated each spectrum with a template spectrum of a hot star, which is dominated by telluric absorption. The resulting velocity is  $v_{\text{center}}$ , the velocity required to shift the spectrum into the geocentric frame. We also computed  $v_{\text{corr}}$ , the correction required to shift from the geocentric to the heliocentric frame. The final heliocentric velocity of the star is  $v_{\text{helio}} = v_{\text{obs}} + v_{\text{center}} + v_{\text{corr}}$ .

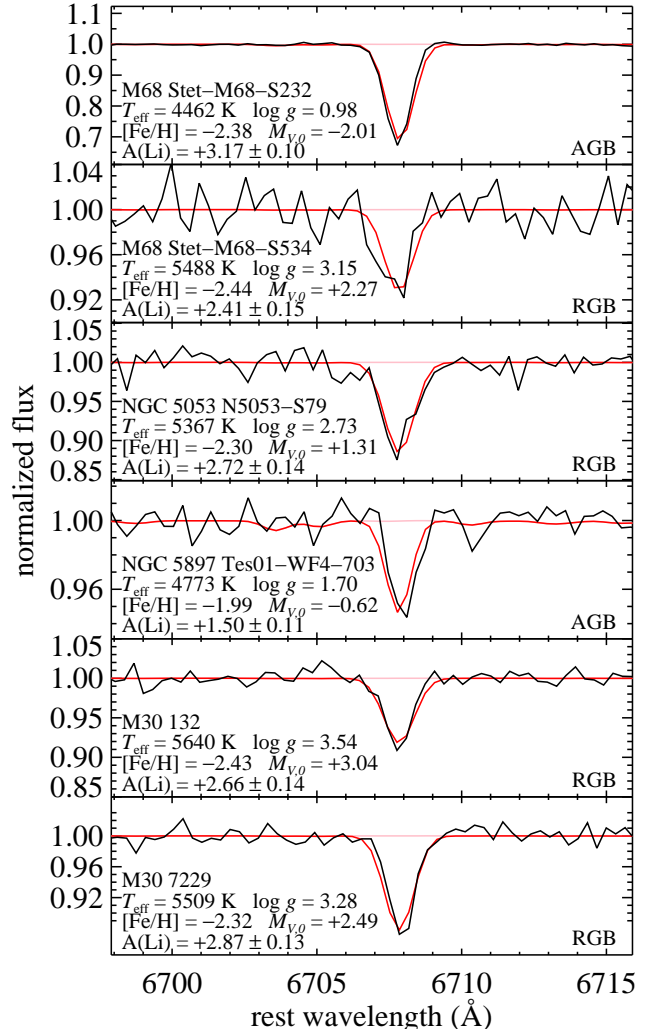


**Figure 2.** DEIMOS spectra (black) of the six Li-rich giants around the  $\text{Li I } \lambda 6707$  absorption line. Best-fit synthetic spectra are shown in red. The pink lines show synthetic spectra with no Li. Each panel gives the star’s host cluster, the star’s name, temperature, gravity, metallicity, luminosity, and NLTE-corrected Li abundance.

#### 3.2. Atmospheric Parameters

We measured  $T_{\text{eff}}$  and  $[\text{Fe}/\text{H}]$  in the same manner as Kirby et al. (2008, 2010). This section summarizes the procedure. First, we shifted the spectrum into the rest frame, removed telluric absorption by dividing by the spectrum of a hot star, and divided by the continuum, approximated by a spline with a breakpoint spacing of  $100 \text{ \AA}$ . Next, we searched for the best-fitting synthetic spectrum among a large grid of spectra computed with MOOG (Snedden 1973) and ATLAS9 model atmospheres (Kurucz 1993; Sbordone 2005).

We estimated initial guesses at  $T_{\text{eff}}$  and surface gravity,  $\log g$ , by comparing the star’s color and magnitude to model isochrones shifted by the distance modulus of its respective GC. In searching the grid,  $T_{\text{eff}}$  was allowed to vary in a range around the photometrically determined value, but  $\log g$  was fixed at the photometric value. On the other hand, no restrictions were imposed on  $[\text{Fe}/\text{H}]$ .

We made “first draft” measurements of  $T_{\text{eff}}$  and  $[\text{Fe}/\text{H}]$  by minimizing  $\chi^2$  between the observed and synthetic

spectra. We refined these measurements by using the best-fit synthetic spectrum to improve the continuum determination. We repeated this iterative continuum refinement until  $T_{\text{eff}}$  and  $[\text{Fe}/\text{H}]$  changed by a negligible amount between iterations. The values of  $T_{\text{eff}}$  and  $\log g$  at the end of the last iteration were regarded as the final measurements.

### 3.3. Membership

We considered only stars that are members of our sample of GCs for the purposes of this project. Our measurements of atmospheric parameters are valid only for member stars because we used model isochrones to estimate  $T_{\text{eff}}$  and  $\log g$ . The measurements are not valid for non-member stars at unknown distances.

First, we removed duplicate spectra. Where a star was observed multiple times on different slitmasks, we kept the measurement with the lowest estimate of error on  $[\text{Fe}/\text{H}]$ , which is essentially a S/N criterion. We removed 437 duplicate spectra.

Second, we eliminated any stars that were obviously non-members or non-giants based on their positions in the CMD. Although the slitmasks were designed to avoid non-members, some obvious non-members were placed on the slitmask merely to fill it with targets. We drew a generous CMD selection region around the stellar locus and flagged stars outside of the region as non-members. Figure 1 shows some of these non-members as crosses. We also eliminated non-giant stars by imposing a cut on surface gravity:  $\log g < 3.6$ .

Third, we restricted the member list on the basis of radial velocity. We estimated the cluster’s mean velocity,  $\langle v_{\text{helio}} \rangle$ , and velocity dispersion,  $\sigma_v$ , by calculating the mean velocity of all stars within  $40 \text{ km s}^{-1}$  of the median velocity. We compiled a list of all stars that satisfied  $|v_{\text{helio}} - \langle v_{\text{helio}} \rangle| < 2.58\sigma_v$  (99% of all stars in a Gaussian velocity distribution). From this list, we re-computed  $\langle v_{\text{helio}} \rangle$  and  $\sigma_v$ . The member list includes only those stars that have  $|v_{\text{helio}} - \langle v_{\text{helio}} \rangle| - \delta v < 3\sigma_v$ , where  $\delta v$  is the uncertainty on the radial velocity. In other words, any star whose  $1\sigma$  velocity error bar overlapped the  $3\sigma_v$  membership cut was allowed as a member. Although the different criteria for stars used in the computation of  $\sigma_v$  versus the member list may seem capricious, we found from examining the velocity histograms that this procedure reliably identified stars in the GC’s velocity peak.

Finally, we restricted the member list on the basis of  $[\text{Fe}/\text{H}]$ . The procedure was nearly identical to the velocity membership criterion. The mean metallicity,  $\langle [\text{Fe}/\text{H}] \rangle$ , and metallicity dispersion,  $\sigma([\text{Fe}/\text{H}])$ , were computed from all stars in the cluster. Then, these values were re-computed from a more restricted list:  $|\langle [\text{Fe}/\text{H}] \rangle - [\text{Fe}/\text{H}]| < 2.58\sigma([\text{Fe}/\text{H}])$  and  $[\text{Fe}/\text{H}] < -0.5$ . With these refined values, the final membership list was those stars with  $|\langle [\text{Fe}/\text{H}] \rangle - [\text{Fe}/\text{H}]| - \delta[\text{Fe}/\text{H}] < 3\sigma([\text{Fe}/\text{H}])$ , where  $\delta[\text{Fe}/\text{H}]$  is the uncertainty on  $[\text{Fe}/\text{H}]$ .

### 3.4. Li Abundance

We measured Li abundances by spectral synthesis of the  $\text{Li I } \lambda 6707$  doublet. We compiled a line list (Table 3) of absorption lines in the region  $6697\text{--}6717 \text{ \AA}$ . The Li absorption lines come from Hobbs et al.’s (1999) list.

**Table 3**  
Line List

| Wavelength ( $\text{\AA}$ ) | Species           | EP (eV) | $\log(gf)$ |
|-----------------------------|-------------------|---------|------------|
| ...                         | ...               | ...     | ...        |
| 6707.752                    | Sc I              | 4.049   | -2.672     |
| 6707.7561                   | <sup>7</sup> Li I | 0.000   | -0.4283    |
| 6707.7682                   | <sup>7</sup> Li I | 0.000   | -0.2062    |
| 6707.771                    | Ca I              | 5.796   | -4.015     |
| 6707.799                    | CN                | 1.206   | -1.967     |
| 6707.9066                   | <sup>7</sup> Li I | 0.000   | -1.5086    |
| 6707.9080                   | <sup>7</sup> Li I | 0.000   | -0.8069    |
| 6707.9187                   | <sup>7</sup> Li I | 0.000   | -0.8069    |
| 6707.9196                   | <sup>6</sup> Li I | 0.000   | -0.4789    |
| 6707.9200                   | <sup>7</sup> Li I | 0.000   | -0.8069    |
| ...                         | ...               | ...     | ...        |

**References.** — Lithium lines are from Hobbs et al. (1999). Other lines are from Kirby et al. (2008), which is compilation of atomic lines from VALD (Kupka et al. 1999) and molecular lines from Kurucz (1993).

**Note.** — Wavelengths are in air. (This table is available in its entirety in a machine-readable form in the online journal. A portion is shown here for guidance regarding its form and content.)

Other lines are from Kirby et al.’s (2008) compilation from VALD (for neutral and ionized atoms, Kupka et al. 1999) and Kurucz (for molecules, 1993). The Li lines are separated by isotope (<sup>6</sup>Li and <sup>7</sup>Li).

We prepared the spectrum by performing a local continuum correction around  $\text{Li I } \lambda 6707$ . We used MOOG and Kirby’s (2011) grid of ATLAS9 model atmospheres to compute a synthetic spectrum devoid of Li. The atmospheric parameters ( $T_{\text{eff}}$ ,  $\log g$ ,  $[\text{Fe}/\text{H}]$ ) were tailored to each star following the procedure in Section 3.2. The microturbulent velocity ( $\xi$ ) was calculated based on a calibration between  $\xi$  and  $\log g$  (Kirby et al. 2009). We divided the observed spectrum by this model. We fit a straight line with variable slope and intercept to the residual in the wavelength range  $6697\text{--}6717 \text{ \AA}$ , but excluding the Li doublet ( $6705.7\text{--}6709.9 \text{ \AA}$ ). This linear fit comprised the local continuum correction, by which we divided the observed spectrum.

We measured  $A(\text{Li})$  in the observed spectrum by minimizing  $\chi^2$  between the continuum-refined, observed spectrum and a model spectrum. The only free parameter in the fit was  $A(\text{Li})$ . We minimized  $\chi^2$  with the Levenberg–Marquardt IDL code MPFIT (Markwardt 2012). This required computing many spectral syntheses with MOOG, which we did in the same manner as for the Li-free spectrum described in the previous paragraph.

We set the <sup>7</sup>Li/<sup>6</sup>Li isotopic ratio to 30. Although  $\text{Li I } \lambda 6707$  spectra modeled with 3D, NLTE model atmospheres show no detectable <sup>6</sup>Li (Lind et al. 2013), a <sup>7</sup>Li/<sup>6</sup>Li ratio of  $\sim 30$ —while not an accurate representation of the atmospheric composition—gives the best-fitting line shape in a 1D, LTE spectral synthesis (Smith et al. 1998), such as ours. Our results are nearly insensitive to this choice because the resolution of our spectra is smaller than the isotopic splitting of the Li doublet.

We took the  $1\sigma$  error on  $A(\text{Li})$  to be the value by which  $A(\text{Li})$  needed to change in order to raise  $\chi^2$  by 1 from the

minimum  $\chi^2$ . For spectra with  $S/N > 300 \text{ pixel}^{-1}$ , this estimate of the error could be even smaller than 0.01, which is unrealistically low because it does not account for systematic error, such as imperfections in the spectral model. We imposed a minimum error of 0.1 dex by adding 0.1 dex in quadrature with the statistical error.

Most of the stars had no detectable Li. For these stars, the  $\chi^2$  contour flattened to a constant value at low  $A(\text{Li})$ . We computed  $2\sigma$  upper limits as the value of  $A(\text{Li})$  corresponding to an increase in  $\chi^2$  of 4 above the minimum  $\chi^2$ . We found this value using a truncated Newton minimization method.<sup>11</sup>

We examined the spectrum of every Li doublet to confirm that the measurement of  $A(\text{Li})$  or its upper limit is valid. We plotted the best-fitting synthetic spectrum over the continuum-corrected observed spectrum. If the fit appeared to fail, then we removed the spectrum from our sample. Common reasons for failure included single-pixel noise spikes (possibly due to cosmic rays) and badly placed continuum measurements due to spectral artifacts. We also flagged every spectrum with a convincing detection of Li. Although we technically measured  $A(\text{Li})$  for every spectrum, we present upper limits for those spectra with unconvincing detections.

Lind et al. (2009a) computed corrections to  $A(\text{Li})$  to counteract deficiencies from the assumption of local thermodynamic equilibrium (LTE) in computing synthetic spectra. The non-LTE (NLTE) correction depends on the LTE lithium abundance and stellar parameters, like  $T_{\text{eff}}$  and  $\log g$ . Lind et al. provided convenient tables to compute NLTE corrections for most cool stars. All of the values of  $A(\text{Li})$ , including upper limits, in the text, figures, and tables in this paper have these NLTE corrections applied. We linearly extrapolated the correction for stars with stellar parameters outside of the range of Lind et al. (2009a)’s tables.

Table 4 gives Li measurements or  $2\sigma$  upper limits for our sample. The table also identifies whether the star fell in the RGB or AGB selection window. Non-members and stars that were removed from the sample upon visual inspection are not shown in the table. The table gives the six Li-rich giants first, followed by all other stars in order of right ascension. The photometric magnitudes and colors are corrected for extinction and reddening.

#### 4. LI ENHANCEMENT

In this section, we quantify the number of Li-rich giants in our sample. To do so, we establish a quantitative definition for “Li-richness.” We also separate the statistics on Li-richness by stellar evolutionary state (RGB or AGB).

##### 4.1. Defining “Li-Rich”

In order to define “Li-rich,” we examine what it means to be “Li-normal.” The definition should depend on the star’s luminosity because surface Li is progressively depleted as the star ascends the RGB. For example, a giant with  $A(\text{Li}) = 1.1$  and  $M_V = +1$  would not be Li-rich, but stars with  $M_V < 0$  begin a phase of Li destruction at the luminosity function bump (in contrast with *dilution* at

the first dredge-up). As a result, a star with  $A(\text{Li}) = 1.1$  and  $M_V = -2$  would be Li-rich.

Lind et al. (2009b) conducted the definitive study of Li in GC stars. They measured  $A(\text{Li})$  for hundreds of stars in the metal-poor GC NGC 6397 from  $R = 14,000$ , high-S/N VLT/FLAMES spectroscopy. Figure 3 shows their measurements in red. The main sequence stars at  $M_V > +3.3$  have a constant  $A(\text{Li}) = 2.3$ . The first dredge-up begins at  $M_V = +3.3$  and depletes  $A(\text{Li})$  to 1.1. The Li remains briefly untouched until the luminosity function bump at  $M_V = 0.0$ , which further depletes Li to an undetectable level.

Our DEIMOS spectra have lower spectral resolution than Lind et al.’s FLAMES spectra. Consequently, we did not detect Li in the majority of our stars. Those stars with detections also have larger  $A(\text{Li})$  uncertainties than the FLAMES measurements. The DEIMOS detections tend to be for stars with larger  $A(\text{Li})$  at fixed  $M_V$  than the FLAMES detections. That is why most of our detections of Li trace the upper envelope of the NGC 6397 data. We have detected Li only in those stars with upward fluctuations in  $A(\text{Li})$  due to intrinsic variation in the cluster or, more likely, random noise in the DEIMOS spectra.

We also quantified what it means to be Li-normal by coadding DEIMOS spectra of RGB stars in six bins of  $M_V$ . The least luminous bin was  $M_V > +2$ , and the most luminous bin was  $M_V < -2$ . The other four bins were 1 mag wide in the range  $+2 > M_V > -2$ . In each bin, we coadded all RGB spectra (excluding the AGB) that do not satisfy the Li-rich criterion (Equation 6). We did not include spectra that we identified in Section 3.4 to be problematic. The spectra were interpolated onto a common wavelength array and coadded with inverse variance weighting. We also averaged  $M_V$  and atmospheric parameters in each bin, weighting by the median inverse variance within 10 Å of Li I  $\lambda 6707$ . We measured  $A(\text{Li})$ , treating the coadded spectrum as a single spectrum with a single  $T_{\text{eff}}$ ,  $\log g$ , and  $[\text{Fe}/\text{H}]$ , which were fixed at the weighted average values for all the spectra in the bin.

Figure 4 shows the coadded spectra. Most absorption lines become stronger with increasing luminosity (note the increasing  $y$ -axis range) because  $T_{\text{eff}}$  decreases with increasing luminosity on the RGB. However, Li I  $\lambda 6707$  becomes weaker because Li is depleted with decreasing  $T_{\text{eff}}$ . Figure 3 compares our coaddition measurements of  $\langle A(\text{Li}) \rangle$  (green) to individual stars in NGC 6397 (red). Except for the  $\langle M_{V,0} \rangle = -0.4$  bin, the green points lie in the midst of the red points. The bin with  $\langle M_{V,0} \rangle = -0.4$  shows a likely spurious absorption feature at 6702 Å, which pushes up the continuum. Therefore, our measurement of  $A(\text{Li})$  might be slightly low in this bin.

The high-quality NGC 6397 data along with our coadded DEIMOS data define a clear trend of  $A(\text{Li})$  with  $M_V$ . We drew a boundary in Figure 3 along the upper envelope of our measurements. The following equation defines the boundary:

$$A(\text{Li}) = \begin{cases} 2.60 & M_V \geq +2.7 \\ 1.50 + \frac{0.33}{3.0 - M_V} & +2.7 > M_V > -0.2 \\ 1.76 + 0.79 M_V & M_V \leq -0.2 \end{cases} \quad (6)$$

Six Li detections fall above the boundary. Although

<sup>11</sup> TNMIN, an IDL code by C. Markwardt (<http://cow.physics.wisc.edu/~craigm/idl/idl.html>).

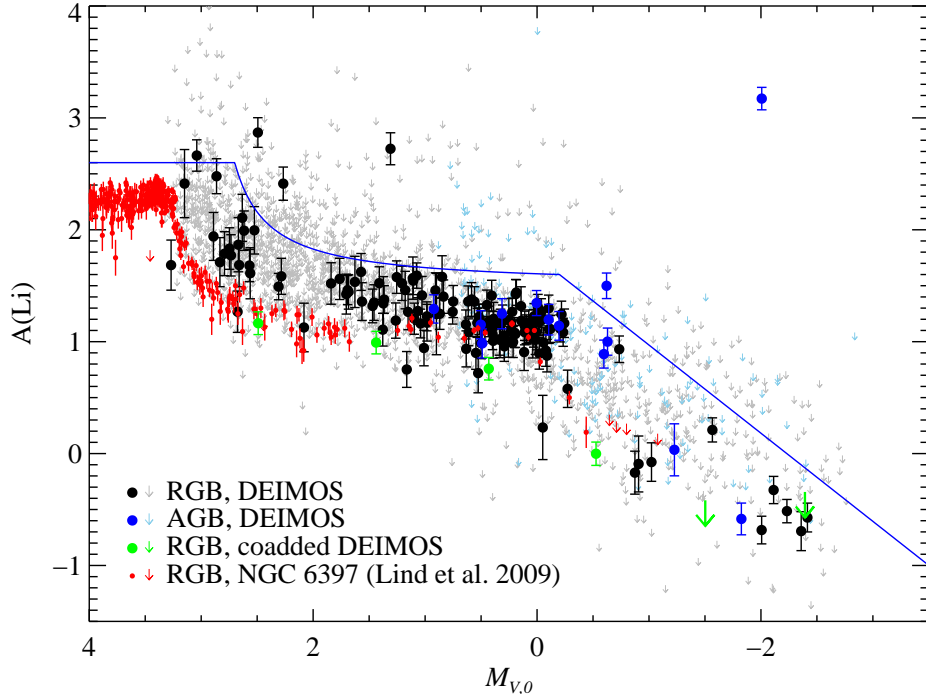


**Figure 3.** NLTE-corrected Li abundances versus absolute magnitude. Our DEIMOS detections of Li are shown as black (RGB) and blue (AGB) points. Upper limits are shown in gray (RGB) and faded blue (AGB). For comparison, high-resolution spectroscopic measurements of Li in the GC NGC 6397 (Lind et al. 2009b) and DEIMOS spectra of red giants coadded in bins of  $M_{V,0}$  are shown in red and green, respectively. The blue curve (Equation 6) separates Li-rich from Li-normal stars.

the exact placement of the boundary is somewhat subjective, Figure 3 shows that there is little ambiguity about which stars are Li-rich. The assignment of Li-rich and Li-normal could be questioned only for the faintest Li-rich star, M30 132. A more rigorous analysis might use multiple levels of Li-richness, such as “Li-normal,” “Li-rich,” and “super Li-rich,” or even a continuously defined “Li-richness” variable. For simplicity, we retain our binary (yes/no) definition, accepting that the Li-richness of M30 132 is ambiguous.

#### 4.2. Li-Rich Frequency

Stars with Li detections above the boundary are considered Li-rich. Stars with Li detections or upper limits below the boundary are Li-normal. Upper limits above the boundary do not indicate whether the star is Li-rich or Li-normal. We calculated the frequency of Li-rich stars as the number of Li-rich stars divided by the total number of detections and “useful” upper limits. If we were to raise the boundary for Li-richness, fewer stars would be considered Li-rich, and more upper limits would be considered useful, both of which would decrease the Li-rich frequency.

Table 5 shows the Li-rich frequency for each GC in our sample and for the combined sample of all 25 GCs. The “Members” column shows stars that passed the membership criteria, regardless of their Li abundances. “Li-rich” shows stars with  $A(\text{Li})$  that exceed the boundary set by Equation 6. “Li-normal” includes stars with detections or upper limits below the boundary. The “Li-Rich Frequency” is  $(\text{Li-Rich})/(\text{Li-Rich} + \text{Li-Normal})$ . The error bars on the frequencies are Poissonian:  $\sqrt{(\text{Li-Rich})}/(\text{Li-Rich} + \text{Li-Normal})$ .

Li-rich giants appear in M68, NGC 5053, M3, NGC 5897, and M30. S232, the more luminous giant in M68 was previously discovered by Ruchti et al. (2011). IV-101, the M3 giant discovered by Kraft et al. (1999), is not in our sample. These clusters do not appear remarkable in any way other than hosting Li-rich giants. Table 5 shows that these clusters have typical luminosities and metallicities.

Two GCs host two Li-rich giants each. M68 has one Li-rich RGB star and one Li-rich AGB star, and M30 has two Li-rich RGB stars. We conducted  $10^6$  random draws of stars from our sample in order to test for the significance of this apparent clustering of Li-rich giants. We drew at least two RGB stars from the same GC in 32% of the trials, and we drew one RGB and one AGB star from the same GC in 46% of the trials. At least two stars of any type were drawn from each of two or more GCs in 11% of the trials. Therefore, clustering of Li-rich giants cannot be ruled out, but the significance is marginal.

The fraction of Li-rich giants across all GCs in our sample is  $(0.3 \pm 0.1)\%$ , notably less than the commonly quoted 1%. The statistics do not include IV-101 in M3 because it was not included in our sample. We obtained a longslit spectrum of this star and confirmed its Li enhancement, but we did so because it was pre-selected to be Li-rich. In order to avoid biasing our results, Table 5 includes only stars that were included in our random sample.

#### 4.3. Stellar Evolutionary State

It is useful to identify the stellar evolutionary phase of the Li-rich giants in order to determine whether they

**Table 5**  
Li-Rich Statistics

| GC             | $M_V$ | [Fe/H] | Members <sup>a</sup> |     | Li-Rich |     | Li-Normal <sup>b</sup> |     | Li-Rich Frequency (%) |               |               |
|----------------|-------|--------|----------------------|-----|---------|-----|------------------------|-----|-----------------------|---------------|---------------|
|                |       |        | RGB                  | AGB | RGB     | AGB | RGB                    | AGB | RGB                   | AGB           | Both          |
| NGC 288        | -6.8  | -1.32  | 106                  | 3   | 0       | 0   | 97                     | 3   | < 1.0                 | < 33          | < 1.0         |
| Pal 2          | -8.0  | -1.42  | 15                   | 1   | 0       | 0   | 3                      | 0   | < 33                  | ...           | < 33          |
| NGC 1904 (M79) | -7.9  | -1.60  | 68                   | 10  | 0       | 0   | 64                     | 10  | < 1.6                 | < 10          | < 1.4         |
| NGC 2419       | -9.4  | -2.15  | 73                   | 10  | 0       | 0   | 18                     | 1   | < 5.6                 | < 100         | < 5.3         |
| NGC 4590 (M68) | -7.4  | -2.23  | 87                   | 5   | 1       | 1   | 80                     | 4   | $1.2 \pm 1.2$         | $20 \pm 20$   | $2.3 \pm 1.6$ |
| NGC 5024 (M53) | -8.7  | -2.10  | 38                   | 6   | 0       | 0   | 23                     | 6   | < 4.3                 | < 17          | < 3.4         |
| NGC 5053       | -6.8  | -2.27  | 39                   | 5   | 1       | 0   | 22                     | 5   | $4.3 \pm 4.3$         | < 20          | $3.6 \pm 3.6$ |
| NGC 5272 (M3)  | -8.9  | -1.50  | 8                    | 5   | 0       | 0   | 8                      | 4   | < 13                  | < 25          | < 8.3         |
| NGC 5634       | -7.7  | -1.88  | 60                   | 1   | 0       | 0   | 42                     | 1   | < 2.4                 | < 100         | < 2.3         |
| NGC 5897       | -7.2  | -1.90  | 216                  | 11  | 0       | 1   | 190                    | 10  | < 0.5                 | $9.1 \pm 9.1$ | $0.5 \pm 0.5$ |
| NGC 5904 (M5)  | -8.8  | -1.29  | 48                   | 3   | 0       | 0   | 48                     | 3   | < 2.1                 | < 33          | < 2.0         |
| Pal 14         | -4.8  | -1.62  | 14                   | 0   | 0       | 0   | 1                      | 0   | < 100                 | ...           | < 100         |
| NGC 6205 (M13) | -8.6  | -1.53  | 55                   | 0   | 0       | 0   | 51                     | 0   | < 2.0                 | ...           | < 2.0         |
| NGC 6229       | -8.1  | -1.47  | 18                   | 1   | 0       | 0   | 13                     | 1   | < 7.7                 | < 100         | < 7.1         |
| NGC 6341 (M92) | -8.2  | -2.31  | 149                  | 2   | 0       | 0   | 142                    | 2   | < 0.7                 | < 50          | < 0.7         |
| NGC 6656 (M22) | -8.5  | -1.70  | 42                   | 0   | 0       | 0   | 42                     | 0   | < 2.4                 | ...           | < 2.4         |
| NGC 6779 (M56) | -7.4  | -1.98  | 49                   | 1   | 0       | 0   | 47                     | 1   | < 2.1                 | < 100         | < 2.1         |
| NGC 6838 (M71) | -5.6  | -0.78  | 32                   | 12  | 0       | 0   | 25                     | 9   | < 4.0                 | < 11          | < 2.9         |
| NGC 6864 (M75) | -8.6  | -1.29  | 105                  | 23  | 0       | 0   | 51                     | 13  | < 2.0                 | < 7.7         | < 1.6         |
| NGC 7006       | -7.7  | -1.52  | 48                   | 5   | 0       | 0   | 20                     | 1   | < 5.0                 | < 100         | < 4.8         |
| NGC 7078 (M15) | -9.2  | -2.37  | 285                  | 42  | 0       | 0   | 261                    | 31  | < 0.4                 | < 3.2         | < 0.3         |
| NGC 7089 (M2)  | -9.0  | -1.65  | 358                  | 11  | 0       | 0   | 317                    | 11  | < 0.3                 | < 9.1         | < 0.3         |
| NGC 7099 (M30) | -7.4  | -2.27  | 119                  | 9   | 2       | 0   | 116                    | 9   | $1.7 \pm 1.2$         | < 11          | $1.6 \pm 1.1$ |
| Pal 13         | -3.8  | -1.88  | 10                   | 0   | 0       | 0   | 5                      | 0   | < 20                  | ...           | < 20          |
| NGC 7492       | -5.8  | -1.78  | 15                   | 4   | 0       | 0   | 10                     | 0   | < 10                  | ...           | < 10          |
| Total          |       |        | 2057                 | 170 | 4       | 2   | 1696                   | 125 | $0.2 \pm 0.1$         | $1.6 \pm 1.1$ | $0.3 \pm 0.1$ |

**References.** — Cluster luminosities and metallicities are from the compilation of Harris (1996, updated 2010) and references therein.

<sup>a</sup> Stars observed with DEIMOS with Li detections or upper limits.

<sup>b</sup> Includes detections of normal Li abundances and useful upper limits (where Li-richness would have been detected).

could have generated the extra Li themselves. Figure 5 shows detail in the CMDs around the Li-rich giants. Four of the Li-rich giants are on the lower RGB, but three giants are bright enough to be AGB stars: M68 S232, M3 IV-101 (not part of our sample), and NGC 5897 WF4-703.

The asymptotic nature of the AGB makes it difficult to assign RGB or AGB status with complete confidence. However, M68 S232 and NGC 5897 WF4-703 lie on the blue side of the giant branches. M3 IV-101 lies on the red side. Therefore, the M68 and NGC 5897 stars are most likely on the AGB, and the M3 star is most likely on the RGB.

Table 5 separates the Li-rich statistics into RGB and AGB. The Li-rich fraction is  $(0.2 \pm 0.1)\%$  for the RGB (not including M3 IV-101) and  $(1.6 \pm 1.1)\%$  for the AGB. The statistics for RGB stars are more certain because we observed over ten times more RGB stars than AGB stars. Although the sample sizes are small, we can estimate the probability that the frequency of Li-rich RGB stars is the same as for Li-rich AGB stars. The Poisson rate ratio test (Lehmann & Romano 2005) returns a  $p$ -value of 0.12 that the rate for Li-richness is the same for the RGB and AGB. Hence, there is an 88% chance that the two populations are different. We consider this to be a marginally significant result.

## 5. DISCUSSION

In this section, we consider the three scenarios for Li enhancement discussed in Section 1: engulfment of a substellar companion, self-generation, and mass transfer.

Although the difference in Li-rich frequencies between the RGB and AGB is marginally significant, different frequencies have significant implications for the origin of Li enhancement. We consider whether each scenario would result in different frequencies for different evolutionary states.

### 5.1. Engulfment of a Substellar Companion

The oldest known exoplanet resides in the GC M4 (Backer et al. 1993; Sigurdsson et al. 2003). However, the exoplanet orbits a pulsar, and it is possible that the pulsar captured the exoplanet from a main sequence star (Sigurdsson 1993). Other than this unusual scenario, exoplanets have limited survivability in GCs due to dynamical interaction (Sigurdsson 1992). Indeed, searches for transiting exoplanets found none in the GCs 47 Tuc and  $\omega$  Cen (Gilliland et al. 2000; Wel Drake et al. 2005, 2008).

If the Li enrichment is due to rotationally induced mixing (Denissenkov & Herwig 2004) caused by an increase in angular momentum from the engulfed companion, then the Li-rich stars should have higher rotation rates. Although there is some evidence for higher rotation rates among metal-rich, Li-rich giants (Guillout et al. 2009), there is no such evidence for metal-poor field stars (Ruchti et al. 2011). Therefore, metal-poor, Li-rich giants in Ruchti et al.'s sample seem not to have generated their Li through rotationally induced mixing.

The low metallicities of GCs also disfavor exoplanet formation. Gas giant exoplanets are increasingly rare around more metal-poor stars (Gonzalez 1997; Santos et al. 2004; Fischer & Valenti 2005) with an oc-

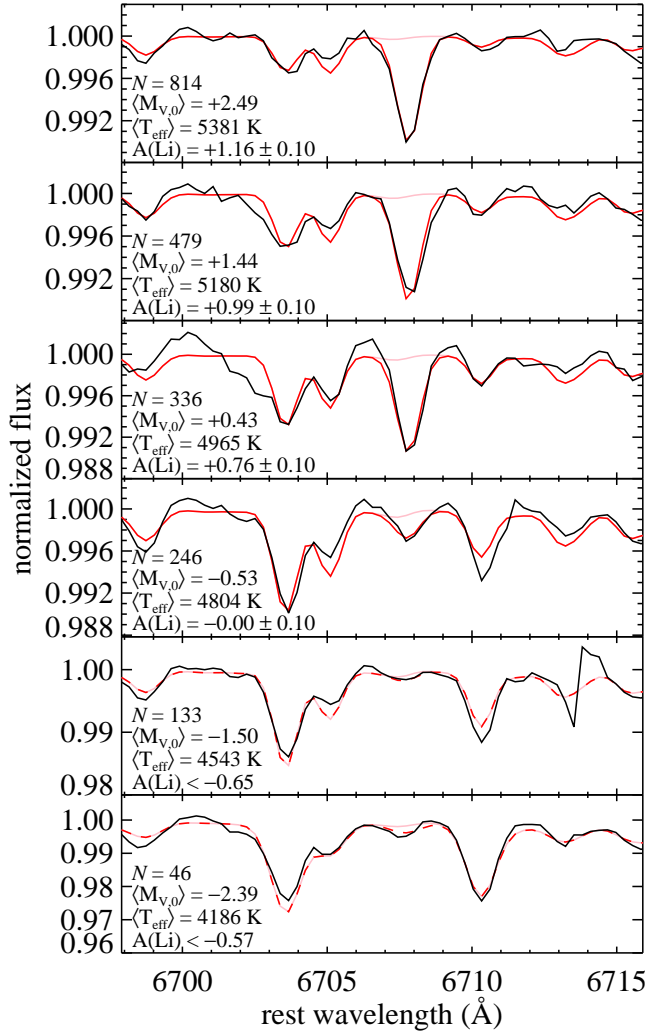


**Figure 4.** Coadded spectra of RGB stars in bins of absolute magnitude ( $M_{V,0}$ ), in order of least luminous (top) to most luminous (bottom). Each panel shows the number of spectra in the coaddition as well as the average  $M_{V,0}$ , average  $T_{\text{eff}}$ , and NLTE-corrected Li abundance. Weak absorption lines not apparent in Figure 2 are visible because the  $y$ -axis ranges of this figure are much smaller. Best-fitting synthetic spectra are shown in red. The red spectra in the bottom two panels show the spectra corresponding to the  $2\sigma$  upper limit on  $A(\text{Li})$  (represented by the broken lines). Synthetic spectra without Li are shown in pink.

currence rate of  $< 1\%$  for  $[\text{Fe}/\text{H}] < -1$  (Johnson et al. 2010). Wang & Fischer (2015) recently showed that gas dwarfs and terrestrial exoplanets are more common around metal-rich stars, although the dependence on metallicity is weaker than for gas giants. (We note that, in contrast to Wang & Fischer 2015, Buchhave et al. 2012 and Neves et al. 2013 found no correlation between host metallicity and the occurrence of planets the size of Neptune or smaller.) All but one (M71) of the GCs in our sample have  $[\text{Fe}/\text{H}] < -1$ . Furthermore, the metallicities of the GCs known to host Li-rich giants are  $[\text{Fe}/\text{H}] = -2.3, -2.3, -2.2, -1.9,$  and  $-1.5$  (NGC 5053, M30, M68, NGC 5897, and M3). The fact that the more metal-rich GCs do not have higher occurrences of Li-rich giants does not favor exoplanets—which tend to occur around metal-rich stars—as the origin of the Li.

The engulfment of a hot Jupiter should occur on the

lower RGB. By the time the star reaches the tip of the RGB, it will have attained close to its maximum radius. Any companion ingestion should happen before then. Thermohaline mixing above the luminosity function bump will destroy any Li acquired from the exoplanet. Therefore, ingestion of a substellar companion cannot explain any Li-rich HB or AGB star. The fact that we found a higher frequency of Li-richness on the AGB than the RGB indicates that companion engulfment cannot be the dominant cause of Li enhancement in giants.

## 5.2. Self-Generation of Lithium

All of the proposed methods for self-generation of Li invoke some version of the Cameron–Fowler conveyor. The conveyor can operate in an intermediate-mass AGB star’s thermal pulse because the convection zone reaches the  $pp$ -II burning region. However, activating the conveyor in an RGB star requires non-canonical mixing.

We have already discussed rotation as one mechanism to induce mixing (Denissenkov & Herwig 2004), but again, the rotation rates of metal-poor, Li-rich field giants are not significantly higher than metal-poor, Li-normal stars (Ruchti et al. 2011). The unremarkable rotation rates in Ruchti et al.’s sample disfavor rotationally induced mixing not only from companion engulfment but also from other sources, including unusually high natal rotation rates. It is possible that the Li-rich giants in GCs have a different distribution of rotation rates than Li-rich giants in the field, but the resolution of our spectra yields line widths ( $45\text{--}50 \text{ km s}^{-1}$ ) that are too large to detect rotation in giants. Regardless, Palacios et al. (2006) were unable to produce Li-rich giants in computational models of rotationally induced mixing.

Other scenarios typically pinpoint one evolutionary stage as the impetus for non-canonical mixing. For example, the mixing could occur at the RGB luminosity function bump (Charbonnel & Balachandran 2000; Palacios et al. 2001) or at the He core flash (Silva Aguirre et al. 2014; Monaco et al. 2014). These scenarios predict that Li-rich stars should appear only at or beyond these evolutionary stages. Red giants reach the bump before the core flash. Therefore, giants that have not reached the bump should not be Li-rich if the Li is to be created at the bump or the He core flash. However, we have found four Li-rich red giants that are much less luminous than the RGB bump. The Li in these stars could not have been created from self-generation at the bump or He core flash.

Even the Li-rich AGB stars in our sample pose problems for the self-generation scenario. Hot bottom burning is effective in creating Li only in AGB stars more massive than  $4 M_{\odot}$  (Sackmann & Boothroyd 1992). The predicted abundance of Li in the atmosphere of a  $1 M_{\odot}$  AGB star with  $[\text{Fe}/\text{H}] = -2.3$  is only  $A(\text{Li}) = 0.5$  (Karakas 2010). However, extra mixing processes, possibly including thermohaline mixing, can induce a Li overabundance in the atmospheres of less massive AGB stars (Cantiello & Langer 2010). The efficacy of this mechanism at producing Li is still very uncertain. The He core flash is also a possible event for inciting extra deep mixing in these AGB stars (Kumar et al. 2011; Silva Aguirre et al. 2014; Monaco et al. 2014).

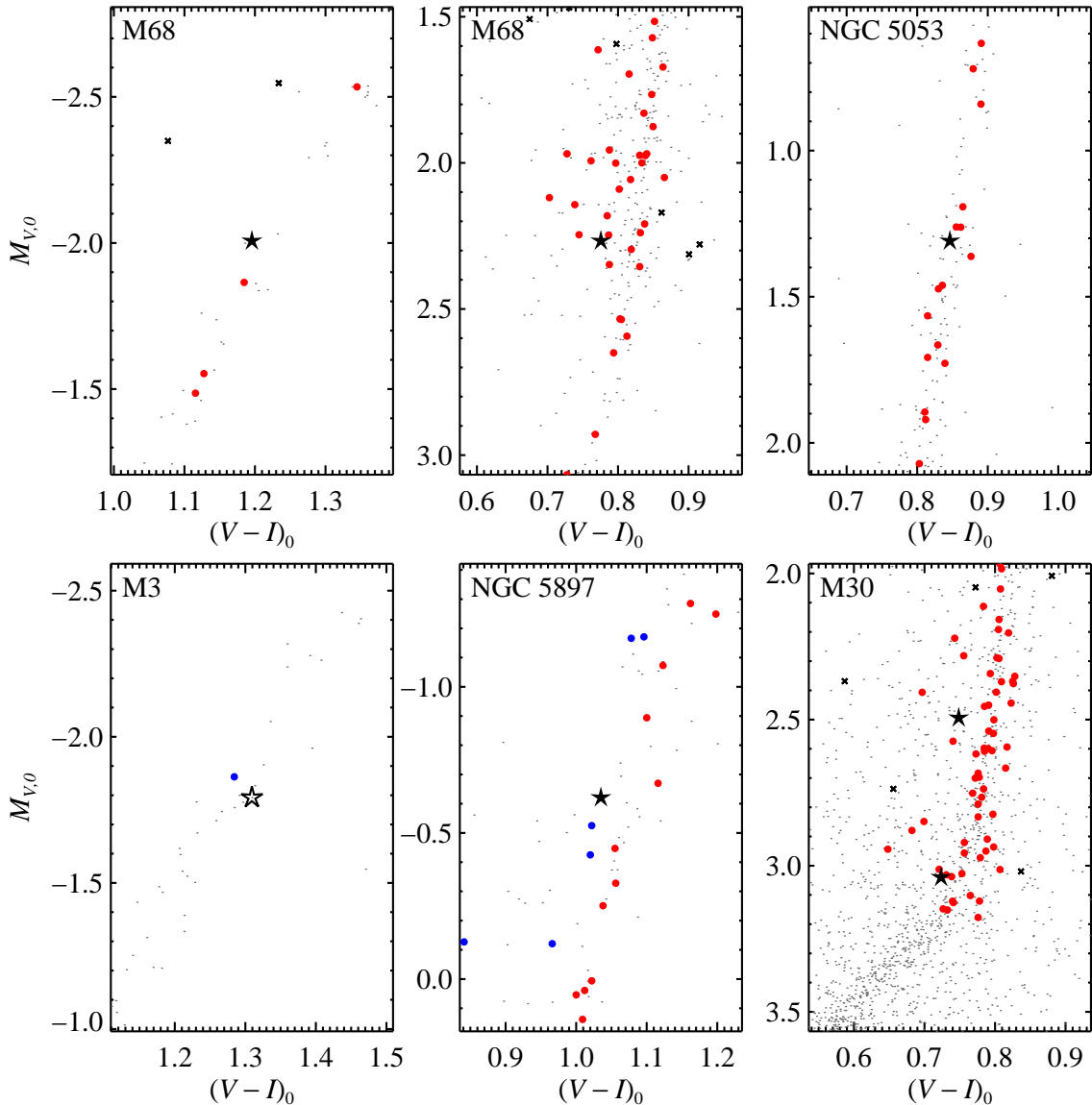


**Figure 5.** Details of the CMDs for the four clusters with Li-rich giants. Although M30 has two Li-rich giants, only one panel is shown because the two stars are close together on the CMD. Because M68 S232 (top left) and NGC 5897 Tes01-WF4-703 (bottom center) lie to the left of the RGB, we identified them as AGB stars. The hollow star indicates the Li-rich giant IV-101 in M3 (Kraft et al. 1999), which is not part of our sample.

### 5.3. Binary Mass Transfer

The only well-understood sites for the generation of large overabundances of Li are intermediate-mass ( $4\text{--}7 M_{\odot}$ ) AGB stars (Cameron & Fowler 1971; Sackmann & Boothroyd 1992; Ventura & D’Antona 2010). These stars did not live long enough to survive in GCs until today. However, an intermediate-mass AGB star could donate its Li to a binary companion. If the companion has a mass less than  $0.8 M_{\odot}$ , it would still be visible in the cluster now. The Li would have been transferred while the recipient was still a dwarf star. This is a favorable configuration for mass transfer because the recipient has a much higher surface gravity than the donor. Although the first dredge-up would deplete some of the Li as the recipient evolved onto the RGB, the dredge-up should deplete the same fraction of surface Li in all stars. Thus, a star enriched in

Li before the dredge-up would still appear enriched in Li after the dredge-up when compared to stars at the same evolutionary stage. The abundance of Li in the atmosphere of an intermediate-mass AGB star can reach up to  $A(\text{Li}) = 4.5$  (Sackmann & Boothroyd 1992), and even higher Li abundances have been observed (de La Reza & da Silva 1995). If the dwarf star acquires that Li abundance early in its life, it could still have  $A(\text{Li}) \approx 3.3$ —even more than the value we observed in our four Li-rich RGB stars—after it passes through the first dredge-up.

The binary frequency in GCs is around 5–10%, but it could have been a factor of two higher before dynamical interactions destroyed binary systems (Ji & Bregman 2013, 2015). Assuming that the binary mass ratio distribution is flat (Boffin 2010) and that the initial binary frequency was 20%, about 1.7% of  $4\text{--}7 M_{\odot}$  stars would have had companions of  $0.8 M_{\odot}$ . In a Kroupa (2001) initial

mass function, 1.3% of 0.08–100  $M_{\odot}$  stars lie in the mass range 4–7  $M_{\odot}$ . Therefore, about  $1.7\% \times 1.3\% = 0.02\%$  of 0.8  $M_{\odot}$  stars once had a companion of 4–7  $M_{\odot}$ . This frequency is an order of magnitude lower than the Li-rich RGB frequency that we observed. Thus, standard hot bottom burning combined with mass transfer could explain about 10% of Li-rich red giants.

The majority of Li-rich giants need to be produced by a different mechanism. The recent discoveries of Li-rich, post-He flash stars (Kumar et al. 2011; Silva Aguirre et al. 2014; Monaco et al. 2014) present another possibility for forming Li-rich giants on the lower RGB. These stars are not as Li-rich as the predictions from hot bottom burning in intermediate-mass AGB stars. If these post-He flash stars were to be the source of Li for stars on the lower RGB, they need to have donated the Li after the recipient completed most of its first dredge-up.

Suppose that all low-mass, metal-poor giants experience one or more short-lived phases of Li enhancement during or after the He core flash. Further suppose that all such giants with companions on the lower RGB will transfer mass to that companion. A 13 Gyr,  $Z = 10^{-4}$  Yonsei-Yale isochrone (Demarque et al. 2004) predicts that a turn-off star had an initial mass of 0.803  $M_{\odot}$  and a star at the RGB bump had an initial mass of 0.812  $M_{\odot}$ . A star at the tip of the RGB experiencing its first He core flash had an initial mass of 0.813  $M_{\odot}$ . If we again adopt a flat binary mass ratio distribution but reduce the binary fraction to 10% (the present rather than the initial value), then about 0.1% of stars at the He core flash should have a binary companion on the lower RGB between the turn-off and the bump. This number is at the lower range of the confidence interval that we measured.

The two main suppositions in this scenario deserve scrutiny. First, we supposed that all GC stars must produce Li on the HB or the AGB. Although this seems like a severe requirement, it circumvents the puzzle of why some giants appear Li-rich and others do not. Instead, all giants experience Li enhancement, but the enhancement is short-lived. This idea—that Li enhancement is rare because it is short-lived—has been suggested several times before (e.g., de la Reza et al. 1997; Charbonnel & Balachandran 2000). If we take our observation of the frequency of Li-rich AGB stars, 1.6%, as representative of all post-He flash stars, then this frequency is equal to the duty cycle of Li enhancement. The post-RGB (HB and AGB) lifetime of a 13 Gyr,  $Z = 10^{-4}$  star is about 130 Myr (Marigo et al. 2008). In our scenario, all such stars spend 2 Myr in a state of Li enhancement.

Second, we supposed that all post-RGB stars with companions on the lower RGB will transfer mass. The lower RGB stars have higher surface gravities than the HB and AGB stars. Therefore, if mass transfer occurs, the HB or AGB star will be the donor. Mass transfer becomes less favorable as the mass difference between the two stars becomes smaller because the secondary star will have a lower surface gravity. After the first dredge-up and before the RGB bump, the mass of the convective envelope in the recipient star is 0.23–0.40  $M_{\odot}$  (Karakas 2003; Karakas & Lattanzio 2014). In order to enrich the star to  $A(\text{Li}) = 2.5$ , a typical value for the Li-rich RGB stars we observed, the star would need to

acquire  $6 \times 10^{-10} M_{\odot}$  of Li. This could be accomplished, for example, by accreting 0.03  $M_{\odot}$  of the envelope of an HB or AGB star that enriched itself to  $A(\text{Li}) = 3.5$ . This amount of mass transfer is not unreasonable. In fact, a single 0.8  $M_{\odot}$  AGB star with  $Z = 10^{-4}$  can lose one quarter of its mass in thermal pulses (Marigo et al. 2008).

However, we also note that low-mass, low-metallicity AGB stars are expected to generate *s*-process elements, like barium (e.g., Karakas et al. 2014). The Ba II  $\lambda 6496$  line is apparent (but blended) in the spectra of all of the Li-rich stars we observed. The line does not appear any stronger than it appears in the Li-normal stars of similar stellar parameters. Thus, it does not seem that either the Li-rich AGB stars or the Li-rich RGB stars are very enhanced in the *s*-process. The lack of *s*-process enrichment in Li-rich GC giants is consistent with metal-rich, Li-rich giants (García-Hernández et al. 2013). These observations demand that the Li be created in the AGB star and/or transferred to the RGB companion before thermal pulses can dredge up large amounts of *s*-process material.

In our scenario, the donor star is no longer visible because it has evolved past the AGB into a white dwarf, too faint to be observed. However, the recipient RGB star is still in orbit around the white dwarf. We predict that Li-rich red giants should show radial velocity variations. Our prediction warrants multi-epoch spectroscopy for those red giants that we found to be Li-rich. We also note that HB or AGB stars that generate Li themselves need not have a binary companion. In fact, only  $\sim 10\%$  of those stars should have a companion (Ji & Bregman 2013, 2015). Therefore, it is not worrisome that Monaco et al. (2014) did not find radial velocity variations around the Li-rich HB star they discovered in Trumpler 5.

## 6. SUMMARY

Although giant stars should deplete Li, some Li-rich giants exist. Some of these giants have Li abundances in excess of the primordial value of the universe, which indicates that the Li is being created, not merely saved from destruction. We examined several proposals for Li enrichment: engulfment of a substellar companion, self-generation, and binary mass transfer.

A GC is the best site to study stellar evolution because it is a single-age, nearly mono-metallic stellar population at a uniform distance. In a survey similar to that of Pilachowski et al. (2000), we searched for Li-rich giants in GCs. The primary difference between our studies is that our sample size was seven times larger, thanks to the multiplexing of Keck/DEIMOS. We measured Li abundances or useful upper limits in 1827 giants across 25 GCs. We defined a luminosity-dependent criterion for Li-richness, and we found that six stars satisfied that criterion. The overall frequency for Li-richness in GCs is  $(0.3 \pm 0.1)\%$ .

Some of the proposed scenarios for Li enrichment predict different frequencies of Li-rich giants at different evolutionary states. Although many non-asteroseismological studies cannot confidently disentangle the RGB and AGB for field stars, we exploited the simplicity of GC stellar populations to assign RGB or AGB identities to each star in our sample. We found that the frequency of

Li-richness is  $(0.2 \pm 0.1)\%$  on the RGB and  $(1.6 \pm 1.1)\%$  on the AGB. A Poisson rate ratio test returns an 88% probability that these two frequencies differ.

We found no correlation between the Li-rich frequency and any property of the GCs, including metallicity. The fact that we found Li-rich giants in extremely metal-poor GCs disfavors exoplanet engulfment as the origin of the Li because exoplanets are not expected to form around extremely metal-poor stars (e.g., Gonzalez 1997; Santos et al. 2004; Fischer & Valenti 2005; Johnson et al. 2010; Wang & Fischer 2015). Furthermore, searches for transiting exoplanets in GCs have found none (Gilliland et al. 2000; Wel Drake et al. 2005, 2008).

Our observations also disfavor self-generation of Li on the RGB. All four of the Li-rich RGB stars we found are on the lower RGB, less luminous than the RGB luminosity function bump. Li-rich RGB stars in GCs have also been found above the bump (Kraft et al. 1999; Smith et al. 1999). Most of the proposed explanations for Li self-generation predict that it will occur at the bump or after the He core flash (e.g., Charbonnel & Balachandran 2000; Silva Aguirre et al. 2014). One exception is rotationally induced mixing (Denissenkov & Herwig 2004), but one study with the spectral resolution to measure rotation rates in metal-poor, Li-rich field giants (Ruchti et al. 2011) found normal rotation rates. Our discovery of four new low-luminosity, Li-rich giants adds to the growing evidence that Li-rich giants can be found at any evolutionary stage (e.g., Monaco et al. 2011; Martell & Shetrone 2013). The wide luminosity range of Li-rich giants rules out most of the proposed scenarios for Li self-generation.

Kumar et al. (2011), Silva Aguirre et al. (2014), and Monaco et al. (2014) found Li-rich giants on the HB, where stars have recently experienced a He core flash. Silva Aguirre et al. supported the identification of their star as a He core-burning, HB star with Kepler asteroseismology. These discoveries could suggest that the He core flash could incite extra deep mixing that activates the Cameron–Fowler conveyor. This explanation applies only to stars on the HB or AGB, not the RGB. However, a post-flash, Li-rich star could transfer Li to a binary companion on the RGB. If all post-RGB stars experience brief phases of Li enhancement and all such stars in binaries transfer mass to their companions, then we expect 0.1% of stars on the lower RGB to be Li-rich. This frequency is consistent with our observations, but it is at the low end of our confidence interval.

Our proposed scenario for explaining Li-rich giants requires the acceptance of several stringent assumptions, but it solves several nagging problems. First, low-luminosity Li-rich giants in GCs do not need to be “special” compared to other Li-normal stars. They merely need to be in a mass transfer binary with a Li-enhanced star. Second, the rarity of the luminous Li-rich giants can be explained by a fast duty cycle of Li enhancement. These stars are “special” only because we happened to observe them during a Li-rich phase. Finally, the Li enhancement does not require the accretion of an exoplanet, whose existence is disfavored in GCs (Gilliland et al. 2000; Wel Drake et al. 2005, 2008; Wang & Fischer 2015).

This manuscript is dedicated to the memory of Bob Kraft. We are grateful to Bob for his mentorship and his inspirational discovery of a Li-rich red giant in M3.

We thank the colloquium audience at Steward Observatory for helpful feedback. We also thank the anonymous referee for a detailed, thoughtful report that improved this article. A.J.Z., J.H., M.G., and R.G. carried out their work through UCSC’s Science Internship Program for high school students. P.G. acknowledges support from NSF grants AST-1010039 and AST-1412648.

We are grateful to the many people who have worked to make the Keck Telescope and its instruments a reality and to operate and maintain the Keck Observatory. The authors wish to extend special thanks to those of Hawaiian ancestry on whose sacred mountain we are privileged to be guests. Without their generous hospitality, none of the observations presented herein would have been possible.

*Facility:* Keck:II (DEIMOS)

## REFERENCES

- Abazajian, K. N., Adelman-McCarthy, J. K., Agüeros, M. A., et al. 2009, *ApJS*, 182, 543
- Adamów, M., Niedzielski, A., Villaver, E., Nowak, G., & Wolszczan, A. 2012, *ApJ*, 754, L15
- An, D., Johnson, J. A., Clem, J. L., et al. 2008, *ApJS*, 179, 326
- Angelou, G. C., Stancliffe, R. J., Church, R. P., Lattanzio, J. C., & Smith, G. H. 2012, *ApJ*, 749, 128
- Anthony-Twarog, B. J., Deliyannis, C. P., Rich, E., & Twarog, B. A. 2013, *ApJ*, 767, L19
- Backer, D. C., Foster, R. S., & Sallmen, S. 1993, *Nature*, 365, 917
- Bellazzini, M., Ferraro, F. R., & Ibata, R. 2002, *AJ*, 124, 915
- Bellazzini, M., Pecci, F. F., Ferraro, F. R., et al. 2001, *AJ*, 122, 2569
- Boesgaard, A. M., Deliyannis, C. P., & Steinhauer, A. 2005, *ApJ*, 621, 991
- Boffin, H. M. J. 2010, *A&A*, 524, A14
- Buchhave, L. A., Latham, D. W., Johansen, A., et al. 2012, *Nature*, 486, 375
- Busso, M., Lambert, D. L., Beglio, L., et al. 1995, *ApJ*, 446, 775
- Cameron, A. G. W. 1955, *ApJ*, 121, 144
- Cameron, A. G. W., & Fowler, W. A. 1971, *ApJ*, 164, 111
- Cantiello, M., & Langer, N. 2010, *A&A*, 521, A9
- Carlberg, J. K., Cunha, K., Smith, V. V., & Majewski, S. R. 2013, *Astronomische Nachrichten*, 334, 120
- Carlberg, J. K., Smith, V. V., Cunha, K., Majewski, S. R., & Rood, R. T. 2010, *ApJ*, 723, L103
- Carlberg, J. K., Smith, V. V., Cunha, K., et al. 2015, *ApJ*, 802, 7
- Carney, B. W., Fry, A. M., & Gonzalez, G. 1998, *AJ*, 116, 2984
- Charbonnel, C., & Balachandran, S. C. 2000, *A&A*, 359, 563
- Charbonnel, C., & Lagarde, N. 2010, *A&A*, 522, A10
- Charbonnel, C., & Zahn, J.-P. 2007, *A&A*, 467, L15
- Chen, Y. Q., Nissen, P. E., Benoni, T., & Zhao, G. 2001, *A&A*, 371, 943
- Coc, A., Goriely, S., Xu, Y., Saimpert, M., & Vangioni, E. 2012, *ApJ*, 744, 158
- Cooper, M. C., Newman, J. A., Davis, M., Finkbeiner, D. P., & Gerke, B. F. 2012, *spec2d: DEEP2 DEIMOS Spectral Pipeline*, astrophysics Source Code Library, ascl:1203.003
- de La Reza, R., & da Silva, L. 1995, *ApJ*, 439, 917
- de la Reza, R., Drake, N. A., da Silva, L., Torres, C. A. O., & Martin, E. L. 1997, *ApJ*, 482, L77
- Delgado Mena, E., Tsantaki, M., Sousa, S. G., et al. 2015, *A&A*, in press, arXiv:1512.05296
- Deliyannis, C. P., Boesgaard, A. M., Stephens, A., et al. 1998, *ApJ*, 498, L147
- Deliyannis, C. P., Demarque, P., & Kawaler, S. D. 1990, *ApJS*, 73, 21
- Demarque, P., Woo, J.-H., Kim, Y.-C., & Yi, S. K. 2004, *ApJS*, 155, 667
- Denissenkov, P. A. 2010, *ApJ*, 723, 563
- 2012, *ApJ*, 753, L3
- Denissenkov, P. A., & Herwig, F. 2004, *ApJ*, 612, 1081
- Denissenkov, P. A., & Weiss, A. 2000, *A&A*, 358, L49
- Dominguez, I., Abia, C., Straniero, O., Cristallo, S., & Pavlenko, Y. V. 2004, *A&A*, 422, 1045
- D’Orazi, V., Angelou, G. C., Gratton, R. G., et al. 2014, *ApJ*, 791, 33

- D’Orazi, V., Gratton, R. G., Angelou, G. C., et al. 2015a, *MNRAS*, 449, 4038
- . 2015b, *ApJ*, 801, L32
- Drake, N. A., de la Reza, R., da Silva, L., & Lambert, D. L. 2002, *AJ*, 123, 2703
- Faber, S. M., Phillips, A. C., Kibrick, R. I., et al. 2003, in *Society of Photo-Optical Instrumentation Engineers (SPIE) Conference Series*, Vol. 4841, *Instrument Design and Performance for Optical/Infrared Ground-based Telescopes*, ed. M. Iye & A. F. M. Moorwood, 1657–1669
- Fischer, D. A., & Valenti, J. 2005, *ApJ*, 622, 1102
- Fu, X., Bressan, A., Molaro, P., & Marigo, P. 2015, *MNRAS*, 452, 3256
- García-Hernández, D. A., Zamora, O., Yagüe, A., et al. 2013, *A&A*, 555, L3
- Gilliland, R. L., Brown, T. M., Guhathakurta, P., et al. 2000, *ApJ*, 545, L47
- Gilliland, R. L., Brown, T. M., Christensen-Dalsgaard, J., et al. 2010, *PASP*, 122, 131
- Gonzalez, G. 1997, *MNRAS*, 285, 403
- Gratton, R., Sneden, C., & Carretta, E. 2004, *ARA&A*, 42, 385
- Gratton, R. G., Carretta, E., & Bragaglia, A. 2012, *A&A Rev.*, 20, 50
- Guillout, P., Klutsch, A., Frasca, A., et al. 2009, *A&A*, 504, 829
- Harris, W. E. 1996, *AJ*, 112, 1487
- Hatzidimitriou, D., Antoniou, V., Papadakis, I., et al. 2004, *MNRAS*, 348, 1157
- Hobbs, L. M., Thorburn, J. A., & Rebull, L. M. 1999, *ApJ*, 523, 797
- Iben, Jr., I. 1968, *ApJ*, 154, 581
- Izzo, L., Della Valle, M., Mason, E., et al. 2015, *ApJ*, 808, L14
- Ji, J., & Bregman, J. N. 2013, *ApJ*, 768, 158
- . 2015, *ApJ*, 807, 32
- Johnson, J. A., Aller, K. M., Howard, A. W., & Crepp, J. R. 2010, *PASP*, 122, 905
- Karakas, A. I. 2003, PhD thesis, Monash University
- . 2010, *MNRAS*, 403, 1413
- Karakas, A. I., & Lattanzio, J. C. 2014, *PASA*, 31, 30
- Karakas, A. I., Marino, A. F., & Nataf, D. M. 2014, *ApJ*, 784, 32
- Kirby, E. N. 2011, *PASP*, 123, 531
- Kirby, E. N., Fu, X., Guhathakurta, P., & Deng, L. 2012, *ApJ*, 752, L16
- Kirby, E. N., Guhathakurta, P., Bolte, M., Sneden, C., & Geha, M. C. 2009, *ApJ*, 705, 328
- Kirby, E. N., Guhathakurta, P., & Sneden, C. 2008, *ApJ*, 682, 1217
- Kirby, E. N., Guhathakurta, P., Simon, J. D., et al. 2010, *ApJS*, 191, 352
- Koch, A., Lind, K., & Rich, R. M. 2011, *ApJ*, 738, L29
- Kraft, R. P., Peterson, R. C., Guhathakurta, P., et al. 1999, *ApJ*, 518, L53
- Kravtsov, V., Alcaíno, G., Marconi, G., & Alvarado, F. 2007, *A&A*, 469, 529
- Kroupa, P. 2001, *MNRAS*, 322, 231
- Kumar, Y. B., & Reddy, B. E. 2009, *ApJ*, 703, L46
- Kumar, Y. B., Reddy, B. E., & Lambert, D. L. 2011, *ApJ*, 730, L12
- Kupka, F., Piskunov, N., Ryabchikova, T. A., Stempels, H. C., & Weiss, W. W. 1999, *A&AS*, 138, 119
- Kurucz, R. 1993, *ATLAS9 Stellar Atmosphere Programs and 2 km/s grid*. Kurucz CD-ROM No. 13. Cambridge, Mass.: Smithsonian Astrophysical Observatory, 1993., 13
- Lattanzio, J. C., Siess, L., Church, R. P., et al. 2015, *MNRAS*, 446, 2673
- Lebzelter, T., Uttenthaler, S., Busso, M., Schultheis, M., & Aringer, B. 2012, *A&A*, 538, A36
- Lehmann, E. L., & Romano, J. P. 2005, *Testing statistical hypotheses*, 3rd edn., *Springer Texts in Statistics* (New York: Springer), xiv+784
- Lind, K., Asplund, M., & Barklem, P. S. 2009a, *A&A*, 503, 541
- Lind, K., Meléndez, J., Asplund, M., Collet, R., & Magic, Z. 2013, *A&A*, 554, A96
- Lind, K., Primas, F., Charbonnel, C., Grundahl, F., & Asplund, M. 2009b, *A&A*, 503, 545
- Marigo, P., Girardi, L., Bressan, A., et al. 2008, *A&A*, 482, 883
- Markwardt, C. 2012, *MPFIT: Robust non-linear least squares curve fitting*, astrophysics Source Code Library, ascl:1208.019
- Martell, S. L., & Shetrone, M. D. 2013, *MNRAS*, 430, 611
- Masseron, T., Johnson, J. A., Lucatello, S., et al. 2012, *ApJ*, 751, 14
- McClure, R. D., Fletcher, J. M., & Nemeč, J. M. 1980, *ApJ*, 238, L35
- Meléndez, J., Casagrande, L., Ramírez, I., Asplund, M., & Schuster, W. J. 2010, *A&A*, 515, L3
- Meléndez, J., Schirbel, L., Monroe, T. R., et al. 2014, *A&A*, 567, L3
- Melo, C. H. F., de Laverny, P., Santos, N. C., et al. 2005, *A&A*, 439, 227
- Monaco, L., Villanova, S., Bonifacio, P., et al. 2012, *A&A*, 539, A157
- Monaco, L., Villanova, S., Moni Bidin, C., et al. 2011, *A&A*, 529, A90
- Monaco, L., Boffin, H. M. J., Bonifacio, P., et al. 2014, *A&A*, 564, L6
- Neves, V., Bonfils, X., Santos, N. C., et al. 2013, *A&A*, 551, A36
- Newman, J. A., Cooper, M. C., Davis, M., et al. 2013, *ApJS*, 208, 5
- Palacios, A., Charbonnel, C., & Forestini, M. 2001, *A&A*, 375, L9
- Palacios, A., Charbonnel, C., Talon, S., & Siess, L. 2006, *A&A*, 453, 261
- Pasquini, L., Koch, A., Smiljanic, R., Bonifacio, P., & Modigliani, A. 2014, *A&A*, 563, A3
- Peterson, R. C., & Cudworth, K. M. 1994, *ApJ*, 420, 612
- Pilachowski, C. A., Sneden, C., & Booth, J. 1993, *ApJ*, 407, 699
- Pilachowski, C. A., Sneden, C., Kraft, R. P., Harmer, D., & Willmarth, D. 2000, *AJ*, 119, 2895
- Pinsonneault, M. H., Deliyannis, C. P., & Demarque, P. 1992, *ApJS*, 78, 179
- Pinsonneault, M. H., Kawaler, S. D., Sofia, S., & Demarque, P. 1989, *ApJ*, 338, 424
- Pinsonneault, M. H., Steigman, G., Walker, T. P., & Narayanan, V. K. 2002, *ApJ*, 574, 398
- Pinsonneault, M. H., Walker, T. P., Steigman, G., & Narayanan, V. K. 1999, *ApJ*, 527, 180
- Plez, B., Smith, V. V., & Lambert, D. L. 1993, *ApJ*, 418, 812
- Richard, O., Michaud, G., & Richer, J. 2005, *ApJ*, 619, 538
- Romano, D., Matteucci, F., Molaro, P., & Bonifacio, P. 1999, *A&A*, 352, 117
- Rosenberg, A., Piotto, G., Saviane, I., & Aparicio, A. 2000, *A&AS*, 144, 5
- Ruchti, G. R., Fulbright, J. P., Wyse, R. F. G., et al. 2011, *ApJ*, 743, 107
- Ryan, S. G., & Deliyannis, C. P. 1995, *ApJ*, 453, 819
- Sackmann, I.-J., & Boothroyd, A. I. 1992, *ApJ*, 392, L71
- . 1999, *ApJ*, 510, 217
- Saha, A., Dolphin, A. E., Thim, F., & Whitmore, B. 2005, *PASP*, 117, 37
- Sandquist, E. L., Bolte, M., Langer, G. E., Hesser, J. E., & de Oliveira, C. M. 1999, *ApJ*, 518, 262
- Santos, N. C., Israelian, G., & Mayor, M. 2004, *A&A*, 415, 1153
- Sbordone, L. 2005, *Memorie della Societa Astronomica Italiana Supplementi*, 8, 61
- Schlegel, D. J., Finkbeiner, D. P., & Davis, M. 1998, *ApJ*, 500, 525
- Siess, L., & Livio, M. 1999, *MNRAS*, 308, 1133
- Sigurdsson, S. 1992, *ApJ*, 399, L95
- . 1993, *ApJ*, 415, L43
- Sigurdsson, S., Richer, H. B., Hansen, B. M., Stairs, I. H., & Thorsett, S. E. 2003, *Science*, 301, 193
- Silva Aguirre, V., Ruchti, G. R., Hekker, S., et al. 2014, *ApJ*, 784, L16
- Simon, J. D., & Geha, M. 2007, *ApJ*, 670, 313
- Smith, V. V., Lambert, D. L., & Nissen, P. E. 1998, *ApJ*, 506, 405
- Smith, V. V., Plez, B., Lambert, D. L., & Lubowich, D. A. 1995, *ApJ*, 441, 735
- Smith, V. V., Shetrone, M. D., & Keane, M. J. 1999, *ApJ*, 516, L73
- Sneden, C. A. 1973, PhD thesis, University of Texas Austin.
- Spite, F., & Spite, M. 1982, *A&A*, 115, 357
- Steinmetz, M., Zwitter, T., Siebert, A., et al. 2006, *AJ*, 132, 1645
- Stetson, P. B. 1987, *PASP*, 99, 191
- . 1994, *PASP*, 106, 250
- . 2000, *PASP*, 112, 925
- . 2011, *DAOPHOT: Crowded-field Stellar Photometry Package*, Astrophysics Source Code Library, ascl:1104.011
- Tajitsu, A., Sadakane, K., Naito, H., Arai, A., & Aoki, W. 2015, *Nature*, 518, 381
- Testa, V., Corsi, C. E., Andreuzzi, G., et al. 2001, *AJ*, 121, 916
- Tucci Maia, M., Meléndez, J., Castro, M., et al. 2015, *A&A*, 576, L10
- VandenBerg, D. A., Bergbusch, P. A., & Dowler, P. D. 2006, *ApJS*, 162, 375
- Ventura, P., & D’Antona, F. 2010, *MNRAS*, 402, L72
- Villaver, E., & Livio, M. 2009, *ApJ*, 705, L81
- Wachlin, F. C., Miller Bertolami, M. M., & Althaus, L. G. 2011, *A&A*, 533, A139
- Walker, A. R. 1994, *AJ*, 108, 555
- Wallerstein, G., & Conti, P. S. 1969, *ARA&A*, 7, 99
- Wang, J., & Fischer, D. A. 2015, *AJ*, 149, 14
- Weldrake, D. T. F., Sackett, P. D., & Bridges, T. J. 2008, *ApJ*, 674, 1117
- Weldrake, D. T. F., Sackett, P. D., Bridges, T. J., & Freeman, K. C. 2005, *ApJ*, 620, 1043

**Table 4**  
Stellar Properties and Lithium Abundances

| GC                         | Name          | RA (J2000)  | Dec (J2000) | Branch | $V_0$ | $(B - V)_0$ | $(V - I)_0$ | $M_V$ | $T_{\text{eff}}$ (K) | $\log g$ (cm s $^{-2}$ ) | [Fe/H]           | $A(\text{Li})$  |
|----------------------------|---------------|-------------|-------------|--------|-------|-------------|-------------|-------|----------------------|--------------------------|------------------|-----------------|
| Li-Rich                    |               |             |             |        |       |             |             |       |                      |                          |                  |                 |
| M68                        | Stet-M68-S232 | 12 39 33.44 | -26 43 13.3 | AGB    | 13.07 | 1.06        | 1.20        | -2.01 | 4462                 | 0.98                     | $-2.38 \pm 0.11$ | $3.17 \pm 0.10$ |
| M68                        | Stet-M68-S534 | 12 39 36.77 | -26 37 57.9 | RGB    | 17.34 | 0.63        | 0.78        | 2.27  | 5488                 | 3.15                     | $-2.44 \pm 0.13$ | $2.41 \pm 0.15$ |
| NGC 5053                   | N5053-S79     | 13 16 38.75 | +17 41 48.2 | RGB    | 17.51 | 0.56        | 0.85        | 1.31  | 5367                 | 2.73                     | $-2.30 \pm 0.11$ | $2.72 \pm 0.14$ |
| NGC 5897                   | Tes01-WF4-703 | 15 17 23.15 | -20 59 42.3 | AGB    | 14.90 | ...         | 1.04        | -0.62 | 4774                 | 1.70                     | $-1.99 \pm 0.11$ | $1.50 \pm 0.11$ |
| M30                        | 132           | 21 40 09.50 | -23 09 46.4 | RGB    | 17.60 | ...         | 0.72        | 3.04  | 5640                 | 3.54                     | $-2.43 \pm 0.12$ | $2.66 \pm 0.14$ |
| M30                        | 7229          | 21 40 18.77 | -23 13 40.4 | RGB    | 17.05 | ...         | 0.75        | 2.49  | 5510                 | 3.28                     | $-2.32 \pm 0.11$ | $2.87 \pm 0.13$ |
| Li-Normal and Upper Limits |               |             |             |        |       |             |             |       |                      |                          |                  |                 |
| NGC 288                    | 206           | 00 52 15.51 | -26 41 04.7 | RGB    | 15.13 | ...         | 0.98        | 0.37  | 4744                 | 2.16                     | $-1.39 \pm 0.11$ | $< 0.42$        |
| NGC 288                    | 1635          | 00 52 20.64 | -26 37 34.7 | RGB    | 17.38 | ...         | 0.82        | 2.62  | 5290                 | 3.26                     | $-1.38 \pm 0.11$ | $< 1.45$        |
| NGC 288                    | 2133          | 00 52 27.93 | -26 37 08.6 | RGB    | 17.16 | ...         | 0.85        | 2.40  | 5228                 | 3.14                     | $-1.28 \pm 0.11$ | $< 1.55$        |
| NGC 288                    | 2228          | 00 52 28.85 | -26 37 04.2 | RGB    | 17.84 | ...         | 0.82        | 3.08  | 5359                 | 3.45                     | $-1.33 \pm 0.11$ | $< 1.71$        |
| ...                        | ...           | ...         | ...         | ...    | ...   | ...         | ...         | ...   | ...                  | ...                      | ...              | ...             |

**Note.** — The table lists Li-rich giants first. The rest of the list is sorted by right ascension. (This table is available in its entirety in a machine-readable form in the online journal. A portion is shown here for guidance regarding its form and content.)

**Table 2**  
DEIMOS Observations

| GC             | Slitmask           | Targets     | UT Date     | Airmass     | Seeing<br>(") | Exposures | Exp. Time<br>(s) |      |
|----------------|--------------------|-------------|-------------|-------------|---------------|-----------|------------------|------|
| NGC 288        | n288               | 119         | 2008 Nov 24 | 1.9         | 0.9           | 3         | 1140             |      |
|                | 28811              | 150         | 2014 Aug 27 | 1.5         | 0.6           | 5         | 5460             |      |
|                | 28812              | 148         | 2014 Aug 28 | 1.5         | 1.0           | 4         | 4800             |      |
|                | 28813              | 148         | 2014 Aug 29 | 1.5         | 0.6           | 4         | 4320             |      |
|                | 28814              | 145         | 2014 Aug 30 | 1.5         | 0.8           | 3         | 4140             |      |
|                | 28815              | 148         | 2014 Aug 31 | 1.5         | 0.8           | 3         | 4320             |      |
| Pal 2          | pal2               | 45          | 2008 Aug 3  | 1.5         | 0.7           | 5         | 940              |      |
| NGC 1904 (M79) | n1904 <sup>a</sup> | 22          | 2006 Feb 2  | 1.4         | ...           | 2         | 600              |      |
|                | ng1904             | 40          | 2009 Feb 22 | 1.4         | 0.9           | 4         | 3600             |      |
|                | 190411             | 98          | 2014 Aug 27 | 2.0         | 0.9           | 3         | 3420             |      |
|                | 190412             | 97          | 2014 Aug 28 | 2.1         | 1.2           | 3         | 4200             |      |
|                | 190413             | 96          | 2014 Aug 29 | 1.9         | 0.8           | 3         | 3360             |      |
|                | 190414             | 96          | 2014 Aug 30 | 1.9         | 1.1           | 3         | 3840             |      |
| NGC 2419       | n2419 <sup>a</sup> | 70          | 2006 Feb 2  | 1.2         | ...           | 4         | 1200             |      |
|                | n2419c             | 94          | 2009 Oct 13 | 1.2         | 0.6           | 2         | 2100             |      |
|                |                    |             | 2009 Oct 14 | 1.2         | 0.5           | 3         | 2700             |      |
|                | n2419b             | 111         | 2012 Mar 19 | 1.1         | 0.7           | 3         | 2700             |      |
|                | NGC 4590 (M68)     | n4590a      | 96          | 2011 Jun 2  | 1.5           | 0.7       | 3                | 2400 |
|                | n4590b             | 96          | 2011 Jun 2  | 1.6         | 0.8           | 3         | 2400             |      |
|                | 459011             | 95          | 2014 Jun 8  | 1.5         | 0.8           | 4         | 4800             |      |
| NGC 5024 (M53) | ng5024             | 40          | 2009 Feb 23 | 1.2         | 0.7           | 2         | 1600             |      |
| NGC 5053       | ng5053             | 40          | 2009 Feb 23 | 1.5         | 0.9           | 3         | 3600             |      |
| NGC 5272 (M3)  | n5272c             | 132         | 2011 Jun 3  | 1.1         | 0.8           | 2         | 960              |      |
| NGC 5634       | n5634a             | 62          | 2011 Jan 30 | 1.2         | 0.7           | 3         | 3700             |      |
|                | n5634b             | 61          | 2011 Jun 2  | 1.1         | 0.7           | 3         | 3907             |      |
| NGC 5897       | 5897a              | 120         | 2011 Aug 6  | 1.4         | 0.8           | 3         | 1800             |      |
|                | 589711             | 117         | 2014 Jun 8  | 1.3         | 0.8           | 3         | 3600             |      |
|                | 589712             | 113         | 2014 Jun 8  | 1.4         | 0.8           | 3         | 3600             |      |
|                | 589713             | 111         | 2014 Jun 29 | 1.3         | 0.8           | 4         | 5400             |      |
|                | 589714             | 114         | 2014 Jun 30 | 1.4         | 0.7           | 5         | 6000             |      |
|                | NGC 5904 (M5)      | ng5904      | 40          | 2009 Feb 22 | 1.1           | 0.6       | 4                | 3180 |
| Pal 14         | pal14a             | 40          | 2011 Aug 6  | 1.3         | 1.2           | 3         | 3960             |      |
| NGC 6205 (M13) | n6205              | 93          | 2007 Oct 12 | 1.4         | ...           | 3         | 900              |      |
| NGC 6229       | 6229a              | 76          | 2011 Jun 3  | 1.2         | 0.7           | 3         | 3900             |      |
| NGC 6341 (M92) | n6341a             | 149         | 2011 Jun 2  | 1.1         | 0.7           | 3         | 1800             |      |
|                | n6341b             | 150         | 2011 Jun 2  | 1.1         | 0.7           | 3         | 1800             |      |
|                | 634111             | 177         | 2014 Jun 8  | 1.1         | 0.8           | 3         | 3600             |      |
|                | 634112             | 174         | 2014 Jun 8  | 1.2         | 0.9           | 3         | 4200             |      |
| NGC 6656 (M22) | n6656b             | 64          | 2009 Oct 13 | 1.5         | 0.8           | 2         | 1800             |      |
|                |                    |             | 2009 Oct 14 | 1.5         | 0.6           | 3         | 2220             |      |
| NGC 6779 (M56) | 677911             | 68          | 2014 Aug 27 | 1.1         | 0.7           | 4         | 4181             |      |
|                | 677912             | 67          | 2014 Aug 27 | 1.0         | 0.8           | 4         | 4200             |      |
|                | 677913             | 87          | 2014 Aug 27 | 1.1         | 0.7           | 4         | 4800             |      |
| NGC 6838 (M71) | n6838              | 105         | 2007 Nov 13 | 1.1         | 0.6           | 3         | 900              |      |
| NGC 6864 (M75) | 6864aB             | 90          | 2011 Aug 5  | 1.4         | 1.1           | 4         | 4800             |      |
|                | 686411             | 120         | 2014 Jun 7  | 1.6         | 1.0           | 4         | 4800             |      |
|                | 686412             | 112         | 2014 Jun 7  | 1.4         | 0.9           | 4         | 4800             |      |
| NGC 7006       | n7006              | 105         | 2007 Nov 15 | 1.0         | ...           | 2         | 600              |      |
|                | 7006a              | 95          | 2011 Jun 3  | 1.1         | 0.7           | 3         | 5040             |      |
| NGC 7078 (M15) | n7078              | 64          | 2007 Nov 12 | 1.0         | ...           | 1         | 300              |      |
|                |                    |             | 2007 Nov 14 | 1.0         | ...           | 2         | 600              |      |
|                | n7078d             | 164         | 2009 Oct 13 | 1.0         | 0.5           | 3         | 2700             |      |
|                | n7078e             | 167         | 2009 Oct 14 | 1.0         | 0.6           | 3         | 2700             |      |
|                | 707811B            | 175         | 2014 Aug 28 | 1.1         | 0.5           | 3         | 3600             |      |
|                | 707812B            | 171         | 2014 Aug 28 | 1.2         | 0.8           | 3         | 3600             |      |
|                | 707813B            | 166         | 2014 Aug 29 | 1.4         | 0.9           | 3         | 3600             |      |
|                | 707814B            | 167         | 2014 Aug 29 | 1.2         | 0.8           | 4         | 4320             |      |
|                | 707815B            | 169         | 2014 Aug 31 | 1.0         | 0.7           | 3         | 3600             |      |
|                | NGC 7089 (M2)      | n7089b      | 91          | 2009 Oct 13 | 1.1           | 0.6       | 3                | 2700 |
|                | 7089c              | 142         | 2011 Jun 3  | 1.1         | 0.9           | 3         | 2340             |      |
|                | 708912             | 154         | 2014 May 28 | 1.2         | ...           | 4         | 7200             |      |
| 708911         | 156                | 2014 May 29 | 1.2         | ...         | 3             | 5400      |                  |      |
| 7089m1         | 145                | 2014 Jun 8  | 1.1         | 0.8         | 4             | 5460      |                  |      |
| 7089m2         | 147                | 2014 Jun 29 | 1.1         | 0.9         | 3             | 3060      |                  |      |
| 708913         | 158                | 2014 Jun 30 | 1.1         | 1.0         | 3             | 2940      |                  |      |
| 708914         | 155                | 2014 Aug 27 | 1.2         | 0.7         | 5             | 5820      |                  |      |
| 708915         | 152                | 2014 Aug 30 | 1.4         | 0.9         | 3             | 3120      |                  |      |
| 708916         | 149                | 2014 Aug 31 | 1.4         | 0.7         | 3             | 4320      |                  |      |
| NGC 7099 (M30) | n7099              | 38          | 2008 Nov 26 | 1.4         | 0.7           | 4         | 1200             |      |
|                | 709911             | 165         | 2014 Aug 29 | 1.6         | 0.8           | 3         | 4320             |      |
|                | 709912             | 157         | 2014 Aug 29 | 1.4         | 0.8           | 3         | 4320             |      |
|                | 709913             | 153         | 2014 Aug 29 | 1.4         | 0.8           | 3         | 4320             |      |
|                | 709914             | 157         | 2014 Aug 30 | 1.4         | 0.8           | 3         | 3600             |      |
|                | 709915             | 156         | 2014 Aug 30 | 1.4         | 0.7           | 3         | 3600             |      |

**Table 2** — *Continued*

| GC       | Slitmask | Targets | UT Date     | Airmass | Seeing<br>(") | Exposures | Exp. Time<br>(s) |
|----------|----------|---------|-------------|---------|---------------|-----------|------------------|
|          | 709916   | 158     | 2014 Aug 30 | 1.5     | 0.7           | 3         | 3600             |
|          | 709917   | 158     | 2014 Aug 31 | 1.4     | 0.7           | 4         | 3900             |
| Pal 13   | pal13    | 33      | 2009 Oct 13 | 1.5     | 0.6           | 2         | 1800             |
|          |          |         | 2009 Oct 14 | 1.5     | 0.7           | 2         | 1722             |
| NGC 7492 | n7492    | 46      | 2007 Nov 15 | 1.3     | ...           | 2         | 420              |

<sup>a</sup> Observations by Simon & Geha (2007).